[American Journal of Science, Vol. 322, January, 2022, P. 28–54, DOI 10.2475/01.2022.02]

CLUMPED ISOTOPE CONSTRAINTS ON WARMING AND PRECIPITATION SEASONALITY IN MONGOLIA FOLLOWING ALTAI UPLIFT

JEREMY K. CAVES RUGENSTEIN*,†, KATHARINA METHNER**,***, TYLER KUKLA***, ANDREAS MULCH**,§, TINA LÜDECKE**,§§, JENS FIEBIG§, ANNE MELTZER§§§, KARL W. WEGMANN‡, PETER ZEITLER§§§, and C. PAGE CHAMBERLAIN***

ABSTRACT. The timing of surface uplift of the Altai Mountains in northern Central Asia—and the climatic consequences—remains controversial. Today, the Altai Mountains cast a substantial rain shadow, effectively separating the western Gobi Desert and steppe from the Siberian Taiga. We take advantage of this stark climatic gradient to trace the interaction of climate and topography in the lee of the Altai. First, we present new water stable isotope data that demonstrate that—along with this climatic gradient—the Altai modify the $\delta^{18}O$ of precipitation via rainout on the leeward side of the range. Second, we present a new paleosol carbonate clumped isotope (Δ_{47}) record that spans much of the Neogene from the immediate lee of the Altai in western Mongolia to address how surface temperatures may have responded to potential uplift during the Neogene. We find that Δ_{47}-derived temperatures have, overall, declined by approximately 7 °C over the course of the Neogene, though the precise timing of this decrease remains uncertain. Third, we pair our Δ_{47} record with previously published stable isotope data to demonstrate that the timing of decreasing temperatures corresponds with long-term stability in paleosol carbonate $\delta^{13}C$ values. In contrast, increases in paleosol carbonate $\delta^{13}C$ values—linked to declining vegetation productivity—are correlated with intervals of increasing temperatures. We speculate that declines in vegetation biomass and leaf area changed the partitioning of latent and sensible heat, resulting in rising surface temperatures during Altai uplift. In contrast, long-term Neogene cooling drove the overall decline in surface temperatures. Reconstructed soil water $\delta^{18}O$ values (based on carbonate $\delta^{18}O$ and Δ_{47} values) remain surprisingly stable over our Neogene record, differing from our expectation of decreasing $\delta^{18}O$ values due to progressive uplift of the Altai Mountains and Neogene cooling. We demonstrate that the shift in precipitation seasonality that likely accompanied Altai uplift obscured any change in lee-side precipitation $\delta^{18}O$ that would be expected from surface elevation change alone.

Key words: Altai, Neogene, Paleoaltimetry, Stable Isotopes, Mongolia

INTRODUCTION

Asia contains one of the most remarkable assemblages of topographic features on the planet. Coincident with much of this topographic diversity are equally impressive climatic gradients, with some of the heaviest rainfall on Earth to the south of the Himalaya whereas, just to the north, lies one of the largest arid regions on our planet. Much work has focused on the history and mechanistic linkages between the uplift

* Department of Geosciences, Colorado State University, Fort Collins, Colorado 80523, USA
** Senckenberg Biodiversity and Climate Research Center, Senckenberg, 60325 Frankfurt, Germany
*** Department of Geological Sciences, Stanford University, Stanford, California 94305, USA
§ Institute of Geosciences, Goethe University, 60438 Frankfurt, Germany
§§ Emmy Noether Group for Hominin Meat Consumption, Max Planck Institute for Chemistry, 55128 Mainz, Germany
§§§ Earth and Environmental Sciences, Lehigh University, Bethlehem, Pennsylvania 18015, USA
‡ Marine, Earth, and Atmospheric Sciences, North Carolina State University, Raleigh, North Carolina 27695, USA
† Corresponding Author: jeremy.rugenstein@colostate.edu

of the Himalaya and Tibetan Plateau region and the development of the Asian monsoon systems and deserts (Hahn and Manabe, 1975; Kutzbach and others, 1993; An and others, 2001; Molnar and others, 2010). However, the uplift history of the Tibetan Plateau remains controversial (Botsyun and others, 2019; Su and others, 2019; Ingalls and others, 2020; Quade and others, 2020) and many of the observed shifts in Cenozoic climate—particularly during the Neogene—are difficult to link directly with pronounced phases of Plateau or Himalayan uplift (Quade and others, 1989; Molnar and others, 2010; Rugenstein and Chamberlain, 2018). In contrast, the many ranges north of the Tibetan Plateau, including the Tien Shan, Altai, Hangay, and Sayan, may have a younger uplift history than the Plateau (Hendrix and others, 1994; Caves and others, 2017) and also exert a profound influence on Asian climate (fig. 1A).

Of these northern ranges, the Altai play a particularly prominent role in modulating East Asian and Northern Hemisphere climate (Roe, 2009; Penny and others, 2010; White and others, 2017). Today, the Altai cast a prominent rain shadow—second only to the Himalaya in Asia—with nearly an order-of-magnitude more precipitation on the windward, northwestern side than on the leeward, eastern side of the range (fig. 1B) (Meyer-Christoffer and others, 2015). Via this rain shadow, the Altai separate the Gobi Desert and steppe from the Siberian taiga by a distance of only ~500 km. On a larger-scale, the Altai's northerly position lends it an outsize importance in modifying the winter-time westerly jet, which reduces storminess across the northern Pacific (Penny and others, 2010; White and others, 2017). Further, the Altai are the largest source of lee cyclones in Asia (Chen and Lazic, 1990; Roe, 2009). In Spring, these cyclones create the tremendous dust storms that traverse East Asia and transport dust as far as western North America (Shao and Dong, 2006; Roe, 2009; Creamean and others, 2013).

Despite the Altai's importance in modulating modern-day Asia climate, the range's role in modifying climate through time remains uncertain, partly because various measures of uplift and climate—derived from exhumation and sedimentation data and proxies of paleoclimate—disagree on the timing of uplift and climate change. Most apatite fission-track (AFT) data record the erosional destruction of the Central Asian Orogenic Belt (CAOB) during the Late Cretaceous (De Grave and others, 2014; McDannell and others, 2018) or indicate renewed exhumation in the latest Paleogene (Yuan and others, 2006; Glorie and others, 2012), though thermal models of AFT data hint at accelerated late Cenozoic cooling (De Grave and others, 2014; Glorie and De Grave, 2016). In western Mongolia, coarsening-upward sedimentation resumes in the late Paleogene after a temporally long unconformity, with growth strata indicative of continued exhumation (Gradzinski and others, 1969; Howard and others, 2003). In contrast, paleoclimate proxy data suggest abrupt changes in climate that could be driven by surface uplift only in the late Miocene or even Pliocene. For example, paleontological data indicates substantially wetter conditions in the Valley of Lakes (western Mongolia; see fig. 1A) in the Pliocene than today (Czyzewski, 1969). Further, paleosol carbonate $\delta^{13}C$ values directly leeward of the Altai increase dramatically beginning in the late Miocene. Although several factors can influence soil carbonate $\delta^{13}C$—including C4 plant abundance, soil respiration, and atmospheric pCO_2 (Cerling, 1999)—this increase was interpreted as a decline in plant productivity and therefore soil respiration rates driven by the establishment of the Altai rain shadow (Caves and others, 2014). However, these changes occur synchronously with global cooling, particularly in the Northern Hemisphere (Herbert and others, 2016), complicating their direct attribution to Altai surface uplift.

One way to test whether late Neogene Altai surface uplift or global cooling drove leeward aridification of western Mongolia would be to use oxygen isotopes ($\delta^{18}O$) of

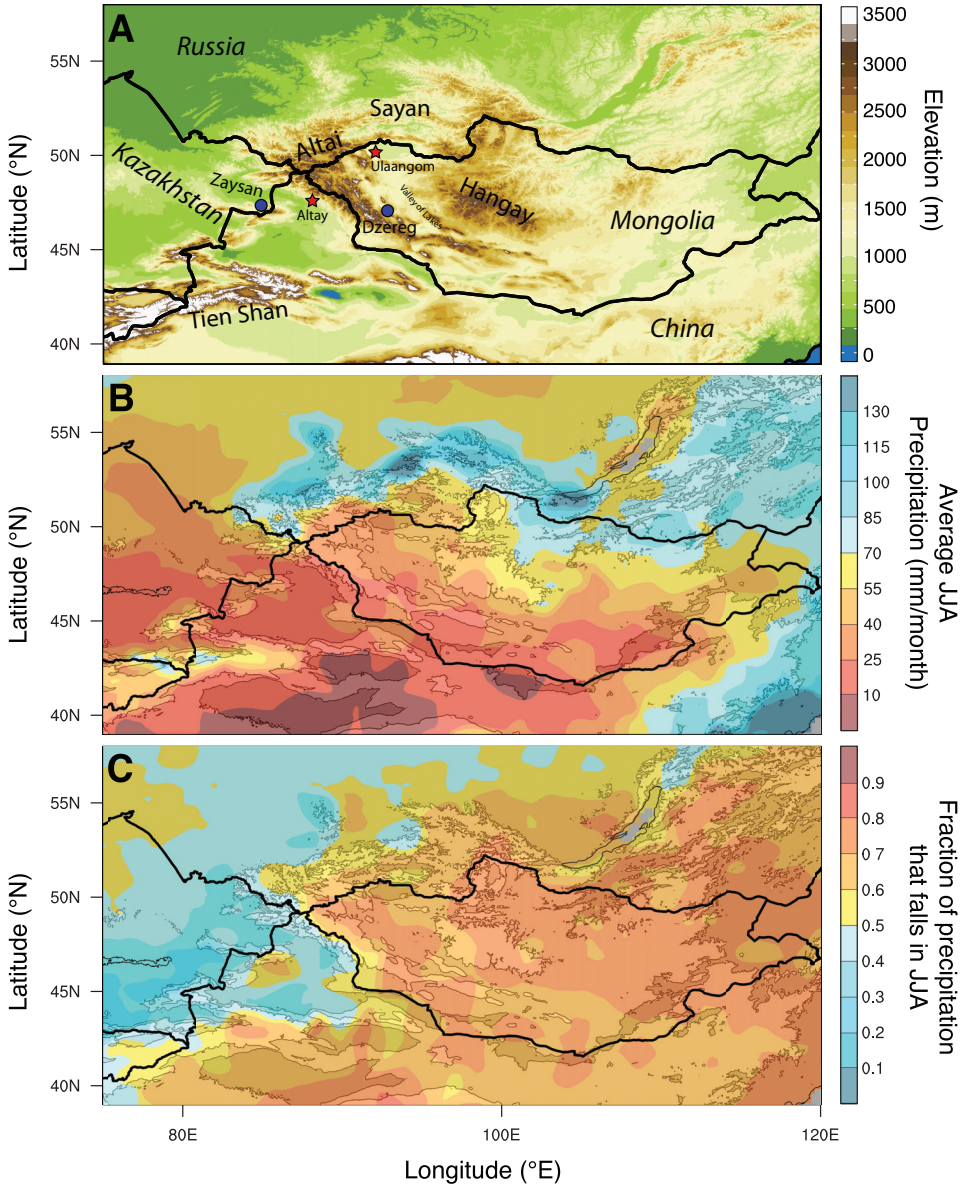

Fig. 1. A) Location map. Blue dots are carbonate stable and clumped isotope sampling sites mentioned in the text. Red stars are locations of precipitation $\delta^{18}O$ stations. B) June, July, August (JJA) precipitation (mm/month). Note the order of magnitude difference in precipitation between the northwest side of the Altai and the leeward, southwest side of the Altai. C) Fraction of annual precipitation that falls during the summer months (JJA). Precipitation data from Meyer-Christoffer and others (2015).

paleosol carbonates. Values of $\delta^{18}O$ in authigenic minerals are frequently used to track the evolution of surface topography in the past, under the assumption that orographic rainout preferentially removes ^{18}O proportional to the height of the mountain range, resulting in lower $\delta^{18}O$ in the lee of the range (Garzione and others, 2000; Poage and Chamberlain, 2001; Rowley and others, 2001; San Jose and others, 2020). Consequently, the $\delta^{18}O$ values of such carbonates should be sensitive to whether the moisture that

reaches western Mongolia has experienced substantial rainout due to passage over the high topography of the Altai. If Altai surface uplift in the late Neogene created the modern-day Altai rain shadow, one would expect increasingly distilled, low $\delta^{18}O$ moisture through time in the lee of the Altai. However, there are few datasets of modern water $\delta^{18}O$ in Mongolia to directly test how the Altai rain shadow impacts modern precipitation $\delta^{18}O$ values. Further, carbonate $\delta^{18}O$ values from lee-side paleosol carbonates do not decline synchronously with the increases in carbonate $\delta^{13}C$ values (Caves and others, 2014). This invariant carbonate $\delta^{18}O$ could reflect stable upwind surface topography. Alternatively, it could reflect countervailing processes that occur concomitantly with changes to the mean upwind topographic elevation of the range that offset any decline in precipitation $\delta^{18}O$ values due to enhanced Altai rainout with uplift. Such processes include *(1)* substantial late Neogene cooling that would change the fractionation of ^{18}O into soil carbonates, or; *(2)* changes in precipitation seasonality that shift the $\delta^{18}O$ of meteoric water that forms soil carbonates.

This contribution, then, has two goals. First, we present 58 new samples of modern, meteoric water $\delta^{18}O$ collected in the lee of the Altai—combined with HYSPLIT modeling of air mass trajectories—to determine if the present-day Altai rain shadow results in lower meteoric water $\delta^{18}O$ on the leeward side of the range. Second, we use clumped isotope (Δ_{47}) paleothermometry on Miocene to Quaternary paleosol carbonates to determine how soil temperatures changed during the late Neogene in the lee of the Altai and, thereby, directly calculate the soil water $\delta^{18}O$ over the same time interval. We use these data to develop a more comprehensive view of how climate in western Mongolia changed during the Neogene and relate these changes to potential tectonic and global climate forcings.

GEOLOGIC AND CLIMATIC SETTING

The Altai is comprised of a series of re-activated fault blocks uplifted along preexisting structures dating to the construction of the Mesozoic Central Asian Orogenic Belt (CAOB) (Cunningham, 1998; Gregory and others, 2018). To the east of the Altai, the Valley of Lakes separates the Altai from the Hangay range, a high-standing, low-relief range that appears to be a long-lasting remnant of the CAOB (McDannell and others, 2018) (fig. 1A). The Valley of Lakes contains abundant but thin Cenozoic growth strata that record erosion off both the Hangay and Altai mountains (Devyatkin, 1981; Traynor and Sladen, 1995). The paleosol carbonate samples analyzed here come from the Dzereg Basin, an internally drained basin bounded by the Mongolian Altai to the west and the Jargalant Naruu range, a 3400 m NW-SE trending transpressional ridge in the Valley of Lakes, to the east.

Here, the thick Mesozoic and thin Cenozoic sequences have been dated largely by biostratigraphy and are described in further detail in Gradzinski and others (1969), Devyatkin (1981), Howard and others (2003), and Caves and others (2014). The approximately 180 m-thick Neogene sequence consists of three distinct stratigraphic units with abundant paleosol horizons rich in authigenic carbonate. We follow the naming convention of Howard and others (2003) for these units: the Miocene-aged Tan Conglomerate Unit, the Pliocene-aged Upper Red Bed Unit, and an unnamed unit comprised of Quaternary alluvial fans. The Tan Conglomerate and Upper Red Bed units contain frequent overbank sediments of fine to medium sands that are strikingly incised by coarser-grained channel units. The channels frequently contain angular clasts that suggest short transport distances, and paleocurrent data (Howard and others, 2003) indicates that the Jargalant Naruu range served as the source for these sediments. The authigenic carbonates are hosted primarily in the overbank sediments, with both nodules (1–3 cm in size) and laterally extensive carbonate-rich Bk horizons frequently cut by overlying channels. The Tan Conglomerate

Unit generally fines upward, whereas the Upper Red Bed Unit contains larger grain sizes, even in the overbank facies. Though no unconformity was observed between the Upper Red Bed and Tan Conglomerate units, there is a substantial angular unconformity with the overlying Quaternary alluvial fans, which blanket the landscape. The duration of this unconformity is unknown. Within these fans, authigenic carbonate appears as well-distributed interstitial cement that has lithified many of these fans.

Climatically, the leeward side of the Altai is strikingly continental. The Valley of Lakes receives approximately 150 mm of precipitation/year, nearly all of which falls during the summer months of June, July, and August (Meyer-Christoffer and others, 2015) (figs. 1B and 1C). Monthly average temperatures vary by more than 40 °C, with summertime temperatures of approximately 25 °C and wintertime temperatures dropping to nearly −20 °C. In contrast, the Altai's windward side receives greater than 1000 mm/year of precipitation, primarily during the spring and fall (fig. 1C). The lack of wintertime precipitation over much of Mongolia results from the exceptionally stable Siberian High, which forms during the late fall and disintegrates in March and April (Aizen and others, 2001).

METHODS

HYSPLIT Modeling

Because the $\delta^{18}O$ of precipitation and meteoric waters are affected by the moisture source and net distillation along the moisture transport pathway (Winnick and others, 2014; Kukla and others, 2019), we use NOAA's HYSPLIT model to determine how moisture that reaches Mongolia interacts with the complex topography in northern Central Asia (Draxler and Hess, 1998). The HYSPLIT model has been frequently used to understand the controls on modern meteoric water $\delta^{18}O$ values and particularly how it applies to reconstructions of $\delta^{18}O$ through time (Oster and others, 2012; Lechler and Galewsky, 2013; Caves and others, 2014; San Jose and others, 2020). Because we are interested in understanding the controls on the spatial distribution of meteoric water $\delta^{18}O$ over Mongolia, we focus on six sites that span Mongolia east-to-west and north-to-south (fig. 2).

To calculate modern back-trajectories, we use climate data output from the Global Data Assimilation System (GDAS), which has an approximately 1° x 1° resolution (Kanamitsu, 1989; Stein and others, 2015) and is the highest-resolution global dataset available to calculate multi-year average trajectories. We compute back-trajectories at 6-hour intervals for 2005 to 2016, resulting in 17,088 back-trajectories. Air parcels are initialized at 1500 m above ground level because the bulk of the moisture is transported in the lower troposphere (Wheeler and Galewsky, 2017). We filter these results for only those trajectories that produce precipitation within 6 hours of the endpoint, though our results are insensitive to variations in this parameter ranging from 1 to 12 hours before the endpoint.

Stable Isotopes of Modern Waters

We collected 58 spring and stream water samples to supplement existing precipitation and surface water $\delta^{18}O$ data from Mongolia (Yamanaka and others, 2007; Kurita and Ichiyanagi, 2008; Caves and others, 2015; Burnik Šturm and others, 2017) (table 1). These waters were all collected during JJA and were sampled opportunistically as part of other projects to characterize the geology and uplift history of the Altai and Hangay (Meltzer and others, 2015). Waters collected in 2013 were measured for $\delta^{18}O$ and δD using 1 ml aliquots on an LGR 24d liquid isotope water analyzer at the Joint Goethe University-SBik-F Stable Isotope Facility, Frankfurt (Germany). Waters collected in 2017 were measured for $\delta^{18}O$ and δD on a Picarro L2120-i isotopic water

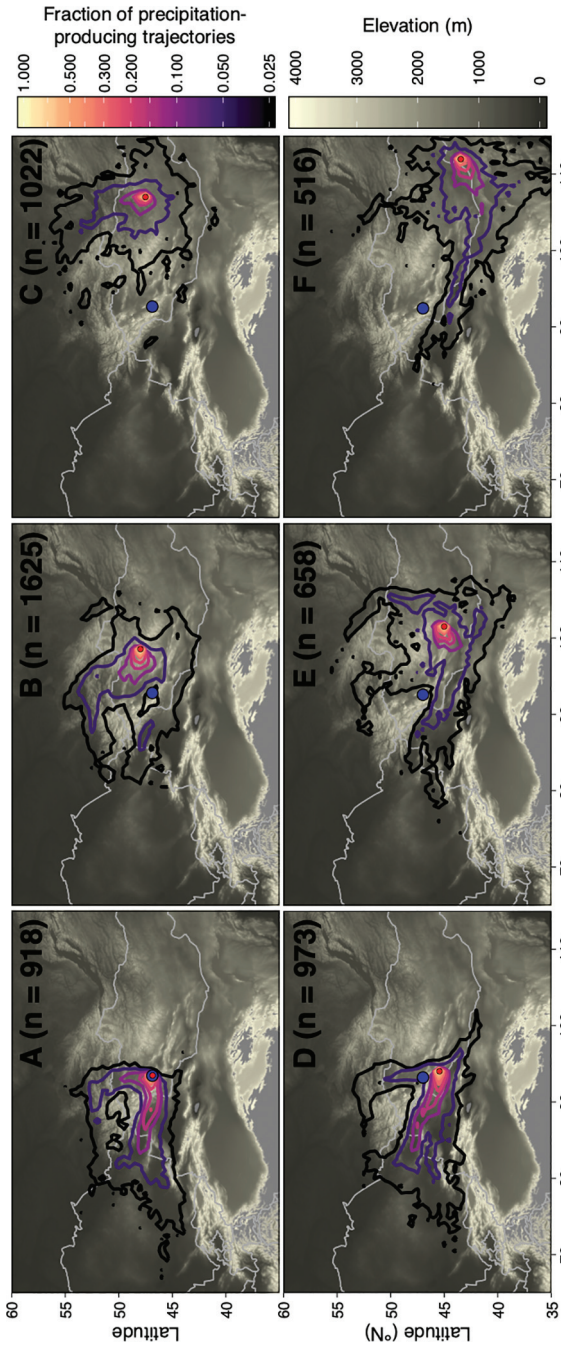

Fig. 2. Two-dimensional histograms of the fraction of precipitation-producing storms between 2005 and 2016 that reach selected sites in Mongolia during JJA (A to C: increasing longitude at high latitudes; D to E: increasing longitude at lower latitudes). Precipitation-producing trajectories are binned by $0.5° \times 0.5°$ to produce density contours (colored lines). Lighter colors indicate a greater fraction of precipitation-producing storms are located within the contour; contour ridges of increasing fraction indicate primary trajectories. *n* indicates the number of precipitation-producing trajectories included in each sub-panel. The blue dot indicates the location of the Dzereg section; the small red dot indicates the starting location of the modeled back-trajectories. Towards the east and south (C, E, and F), a greater fraction of trajectories does not traverse high topography.

TABLE 1

River and stream $\delta^{18}O$ and δD data. All isotopic values are relative to VSMOW. Samples with "–" in the "Day of Year" column were collected in July.

Sample	Latitude (°N)	Longitude (°E)	Year	Day of Year	δD	δD (1σ)	$\delta^{18}O$	$\delta^{18}O$ (1σ)
AM1	44.477	102.426	2013	156	-102.8	0.69	-13.60	0.064
AM2	45.521	96.645	2013	158	-98.9	0.62	-13.75	0.057
AM3	45.792	96.091	2013	159	-160.6	0.90	-21.53	0.074
AM4	47.500	96.885	2013	159	-106.5	0.48	-14.16	0.081
AM5	49.473	98.077	2013	160	-114.3	0.40	-14.72	0.027
AM6	49.560	99.374	2013	161	-138.6	0.33	-18.29	0.052
AM7	48.740	103.612	2013	162	-92.1	0.14	-11.74	0.072
B1	48.022	100.417	2013	157	-83.4	0.52	-10.78	0.038
B10	48.009	98.630	2013	160	-116.2	0.56	-14.95	0.072
B11	47.986	98.557	2013	160	-113.0	0.17	-14.56	0.051
B12	47.740	98.337	2013	160	-106.5	0.37	-13.66	0.048
B13	47.868	98.464	2013	160	-114.8	0.44	-14.75	0.074
B14	47.820	98.825	2013	160	-135.9	0.40	-18.36	0.075
B15	47.827	98.916	2013	160	-104.6	0.39	-13.92	0.042
B16	47.756	100.232	2013	163	-77.5	0.13	-8.98	0.050
B17	47.297	100.036	2013	163	-95.5	0.70	-12.69	0.031
B19	46.239	101.697	2013	167	-81.9	0.44	-11.24	0.096
B2	48.195	99.693	2013	158	-122.0	0.49	-16.29	0.040
B20	46.353	102.121	2013	167	-89.0	0.27	-11.78	0.045
B21	46.537	102.514	2013	168	-89.7	0.30	-11.84	0.048
B22	46.792	102.359	2013	168	-105.7	0.21	-14.53	0.030
B23	46.751	102.327	2013	168	-102.5	0.30	-14.11	0.049
B3	48.220	99.436	2013	158	-106.7	0.31	-14.41	0.053
B4	48.242	99.393	2013	158	-109.1	0.26	-14.18	0.021
B5	48.267	99.396	2013	158	-106.2	0.28	-13.78	0.049
B6	48.314	99.394	2013	158	-124.6	0.58	-16.64	0.063
B7	48.191	99.169	2013	159	-110.1	0.20	-14.34	0.027
B9	48.053	99.075	2013	159	-87.2	0.67	-11.18	0.045
KW1	47.425	103.569	2013	176	-87.6	0.63	-10.78	0.051
KW16	47.102	99.942	2013	183	-108.1	0.28	-15.44	0.018
KW18	46.804	98.003	2013	184	-103.4	0.36	-13.69	0.049
KW19	47.499	97.637	2013	184	-122.3	0.64	-16.49	0.043
KW2	47.453	101.751	2013	177	-99.2	0.12	-13.50	0.059
KW21	46.602	99.975	2013	185	-92.3	0.17	-12.87	0.019
KW22	46.582	99.854	2013	186	-82.3	0.20	-10.87	0.078
KW23	46.660	101.210	2013	187	-89.3	0.27	-12.70	0.033

TABLE 1
(Continued)

Sample	Latitude (°N)	Longitude (°E)	Year	Day of Year	δD	δD (1σ)	$\delta^{18}O$	$\delta^{18}O$ (1σ)
KW24	46.690	101.304	2013	188	-91.8	0.23	-12.48	0.035
KW25	46.768	101.430	2013	189	-99.1	0.19	-13.62	0.025
KW26	46.845	101.533	2013	189	-94.4	0.27	-12.89	0.023
KW3	47.436	100.199	2013	177	-90.3	0.31	-12.43	0.042
KW5	47.270	100.033	2013	178	-99.6	0.19	-13.67	0.030
KW8	47.201	100.102	2013	180	-124.5	0.36	-17.16	0.042
ws1	48.578	98.953	2017	--	-110.9	0.2	-14.79	0.05
ws10	47.452	92.197	2017	--	-98.5	0.1	-13.15	0.07
ws11	46.590	92.289	2017	--	-110.4	0.2	-15.03	0.04
ws11	45.353	90.856	2017	--	-102.6	0.5	-13.98	0.04
ws12	46.104	91.542	2017	--	-107.7	0.3	-14.77	0.03
ws13	45.981	93.267	2017	--	-115.8	0.3	-15.65	0.05
ws14	46.232	93.372	2017	--	-106.8	0.1	-14.74	0.05
ws15	46.311	93.908	2017	--	-94.5	0.1	-13.35	0.07
ws2	49.240	96.417	2017	--	-117.4	0.2	-15.12	0.09
ws3	49.909	92.218	2017	--	-113.9	0.1	-15.66	0.03
ws4	49.126	90.319	2017	--	-111.7	0.4	-15.36	0.07
ws5	48.834	89.196	2017	--	-105.6	0.2	-14.85	0.04
ws6	48.561	88.866	2017	--	-94.0	0.6	-12.19	0.08
ws7	48.898	89.644	2017	--	-99.1	0.2	-13.66	0.07
ws8	48.428	90.399	2017	--	-111.1	0.2	-15.57	0.03
ws9	48.404	90.869	2017	--	-100.2	0.2	-14.14	0.08

analyzer coupled to a Picarro A0211 High Precision Vaporizer at ETH Zurich (Switzerland). Water aliquots of 1 ml were filtered through 0.45 μm disposable membrane filters before injection. At both laboratories, $\delta^{18}O$ values were corrected based on internal lab standards calibrated against VSMOW (Vienna Standard Mean Ocean Water). The analytical precision is typically better than 0.2‰ (2σ) absolute for $\delta^{18}O$ values.

Clumped Isotope Analyses

Carbonate clumped isotope (Δ_{47}) analyses on nine selected carbonate samples, limited to pedogenic nodules and soil calcic (Bk) horizons, from the 160 m thick Mio-Pliocene section in the Dzereg Basin were performed at the Joint Goethe University-Senckenberg BiK-F Stable Isotope Facility, Frankfurt am Main, Germany. Sample powders were prepared using a Dremel in 2012 (originally for stable isotope analysis), and aliquots of these powders were used for clumped isotope analysis. The data were acquired in two analytical sessions. In a first pilot study (that is, in the first analytical session), we analyzed four pedogenic carbonate samples on a ThermoFisher MAT 253 gas-source isotope ratio mass spectrometer (IRMS) dedicated to measurements of atomic masses 44 to 49. During this analytical period, sample preparation and

measurements followed the procedure outlined in Wacker and others (2013, 2014). In brief, pedogenic carbonate powder was digested in >106% phosphoric acid at 90 °C for 30 minutes. The produced CO_2 was purified by passing it through cryogenic traps (–80 °C) before and after passage through a Porapak Q-packed gas chromatography column (–15 °C) to remove traces of hydrocarbons. In the second session, we complemented this initial Δ_{47} data set using HAL (Hofmann's Auto Line) for phosphoric acid digestion of the carbonates at 90 °C, purification of extracted CO_2 and introduction of the cleaned CO_2 to a Thermo Scientific MAT 253plus IRMS for isotopic analysis of the purified CO_2 (Fiebig and others, 2019).

All data is calculated using the [Brand]/IUPAC parameters (Daëron and others, 2016) and is reported in the Carbon Dioxide Equilibrium Scale (CDES) normalized to 25 °C. Alongside samples and internal carbonate standards (ETH1 to ETH4, Carrara marble, aragonitic bivalve *Arctica islandica*; see supplementary table S5, http://earth.eps.yale.edu/%7eajs/SupplementaryData/2022/Rugenstein), CO_2 gases equilibrated at 1000 °C and 25 °C (supplementary tables S1 and S2) were measured to monitor the non-linearity of the mass spectrometer and to determine the empirical transfer functions (ETFs) for the projection of background-corrected Δ_{47} raw data to the CDES (Dennis and others, 2011). During the first analytical session, each sample replicate was analyzed in 10 acquisitions consisting of 10 cycles of reference-sample gas measurements with 20 s integration time each. Background correction was performed according to the protocol outlined by Fiebig and others (2016). During the second session, each sample replicate was analyzed in 13 acquisitions (10 cycles with 20 s integration time each). The negative background was continuously monitored on the m/z 47.5 half cup and subtracted from the measured m/z 47 intensity using an empirically derived scaling factor of −0.988 (as outlined in detail by Bajnai and others, 2018). For the construction of the ETFs we considered the intercepts of background-corrected equilibrated gases and their corresponding thermodynamic equilibrium values (Wang and others, 2004). A 25 to 90 °C acid fractionation factor of 0.088‰ was finally added to ETF-processed Δ_{47} values and clumped isotope temperatures (T) were calculated using the Wang-Dennis processed calibration of Petersen and others (2019):

$$\Delta_{47} = 0.0387 \times \frac{10^6}{T^2} + 0.257 \quad (1)$$

Each sample was typically replicated 4 to 7 times. One sample (Dz-65) was analyzed four times in the first and three times in the second session and yielded identical values within ± 1 standard error of the mean (SE) (table 2). External standard errors (±1 standard error of the mean (SE)) for 4–7 replicate measurements range from ± 0.002‰ to ± 0.014‰. For sample Dz-44, measured in 5 replicates in the second session interval, the 1 SE of 0.002‰ is smaller than the corresponding shot noise limit of 0.003‰ (Merritt and Hayes, 1994). Therefore, we replaced the calculated 1 SE with the shot-noise limit for this sample.

RESULTS

HYSPLIT Modeling Results

HYSPLIT trajectory modeling reveals that most of Mongolia is influenced by westerly moisture, with only the eastern- and southern-most sites influenced by monsoonal moisture from the south (fig. 2). The topography of the Altai, Hangay, and Sayan ranges strongly influences these western moisture trajectories. In western Mongolia, precipitation-producing trajectories rarely traverse the highest portion of the Altai

TABLE 2

Clumped isotope results, carbonate $\delta^{18}O$ and $\delta^{13}C$ from Caves et al. (2014), and reconstructed soil water $\delta^{18}O$ and soil CO_2 $\delta^{13}C$. Listed uncertainties for soil water $\delta^{18}O$ and soil CO_2 $\delta^{13}C$ are calculated using the 1σ of the temperature.

Sample name	Strat. height [m]	Age [Ma]	Sample type	n	$\delta^{18}O$ (VSMOW)	$\delta^{13}C$ (VPDB)	Δ_{47} [CDES 90]	Δ_{47} [CDES 25]	SD Δ_{47}	SE Δ_{47}	Temperature (°C)	1σ Temperature (°C)	Soil Water $\delta^{18}O$ (VSMOW)	Soil CO_2 $\delta^{13}C$ (VPDB)
Dz33	9	Miocene	Nodule	6	18.99	-9.06	0.622	0.710	0.007	0.004	19.3	2.4	-10.55 ± 0.5	-18.61 ± 0.26
Dz35	15	Miocene	Nodule	4	19.59	-8.38	0.628	0.716	0.013	0.010	17.1	4.1	-10.43 ± 0.87	-18.17 ± 0.45
Dz41	36	Miocene	Caliche	5	19.72	-9.45	0.639	0.727	0.008	0.005	13.8	2.4	-11.01 ± 0.52	-19.60 ± 0.26
Dz44	46	Miocene	Caliche	5	20.29	-8.6	0.645	0.733	0.003	0.004	12.0	0.9	-10.85 ± 0.2	-18.95 ± 0.1
Dz51	68	Miocene	Caliche	5	19.9	-10.02	0.652	0.740	0.007	0.004	9.9	1.9	-11.70 ± 0.42	-20.60 ± 0.21
Dz56	94	Miocene	Nodule	4	20.25	-6.78	0.644	0.732	0.009	0.007	12.4	2.7	-10.80 ± 0.59	-17.08 ± 0.3
Dz57	109	Miocene	Caliche	6	21.25	-5.37	0.630	0.727	0.008	0.004	16.5	2.6	-8.95 ± 0.55	-15.22 ± 0.28
Dz61	124	Miocene	Nodule	5	21.04	-6.38	0.638	0.716	0.010	0.006	14.2	3.1	-9.65 ± 0.67	-16.49 ± 0.34
Dz65	142	Pliocene	Caliche	7	20.73	-5.79	0.642	0.730	0.011	0.005	12.8	3.3	-10.25 ± 0.72	-16.05 ± 0.36

and instead split around the high elevations, traveling over the lower topography that connects the Altai and Sayan in the north or the Gobi Altai to the south (figs. 2A and 2D). Moisture that reaches the northwestern flanks of the Hangay often passes over the topography that separates the bulk of the Altai and Sayan ranges (fig. 2B), whereas moisture reaching the southeast flank of the Hangay tends to traverse the Gobi Altai or be sourced from local or more southerly locations (fig. 2B). In northeastern Mongolia, most moisture travels around the Sayan and Hangay and does not traverse high topography at all (fig. 2C). Moreover, in southeastern Mongolia, near the border with China, most moisture appears to be locally generated or from the west or south—potentially from the East Asian Monsoon—again with apparently little interaction with high topography (fig. 2F). Though we plot trajectories that only occur during JJA, the results are not substantially different if all annual trajectories are considered since all sites receive a large fraction of annual precipitation during JJA (fig. 1C). Though we choose 1500 m above ground level as the starting point for the trajectories, the results are also not particularly sensitive to the starting height. At higher starting levels, a greater fraction of precipitation-producing storms passes directly over the Altai, rather than skirting around the northern edge (not shown); nevertheless, these trajectories still traverse the high topography of the Altai.

These HYSPLIT trajectories demonstrate that areas in the western and northwestern portions of Mongolia receive moisture that has experienced flow over relatively high topography. In contrast, areas to the east and south receive moisture that has experienced less direct flow over elevated topography and is increasingly mixed with moisture from the south.

Modern Water Stable Isotopes

The combined meteoric water $\delta^{18}O$ ($\delta^{18}O_{mw}$) values from Mongolia—including newly presented data and data previously published in Caves and others (2015) and Burnik Šturm and others (2017)—range from −7.85 to −21.53‰, with a mean of −13.72 ± 1.93‰ (1σ) (table 1). The local meteoric water line (MWL) of all river/stream stable isotope data has a slope of 6.93 ± 0.13 and an intercept of −7.12 ± 1.81‰; in contrast, the MWL of all river/stream data from across Asia has a slope of 8.28 ±0.05 and an intercept of 12.35 ± 0.73‰ (fig. A1A). Regionally, modern precipitation and river/stream $\delta^{18}O$ data from Asia define a coherent pattern of values decreasing poleward similar to the global pattern of decreasing poleward $\delta^{18}O$ values (Dansgaard, 1964) (gray line in fig. 3B). However, two regions in Asia deviate from this poleward trend: the leeward areas of the Himalayas and the Altai. In both cases, waters collected leeward of these ranges have $\delta^{18}O$ values lower than expected from latitudinally equivalent, non-leeward data (fig. 3B). In map view, waters collected in and around western Mongolia show substantial variability (fig. 3A). Nevertheless, $\delta^{18}O_{mw}$ is lower in the lee of the Altai and over the northwest Hangay, which also receives precipitation that has traversed the high topography of the northern Altai and Sayan (fig. 2). In eastern and southern Mongolia, $\delta^{18}O_{mw}$ values are higher, particularly in the southeastern portion of the Hangay and further to the south and east.

Clumped Isotopes and Reconstructed Soil Water $\delta^{18}O$ and Soil CO_2 $\delta^{13}C$

Carbonate clumped isotope analyses from Dzereg nodules and carbonate-rich Bk horizons yield Δ_{47} values of 0.740 ± 0.007 to 0.710 ± 0.007‰ (±1σ), which translate into temperatures of 9.9 ± 1.9 °C to 19.3 ± 2.4 °C (± 1σ), respectively (table 2). We do not detect any differences between Δ_{47} values of nodules and soil Bk horizons. Overall, Δ_{47}-temperatures show a trend towards lower temperatures from the bottom to the top of the section (fig. 4). Within the lower part of the section (9–68 m), there

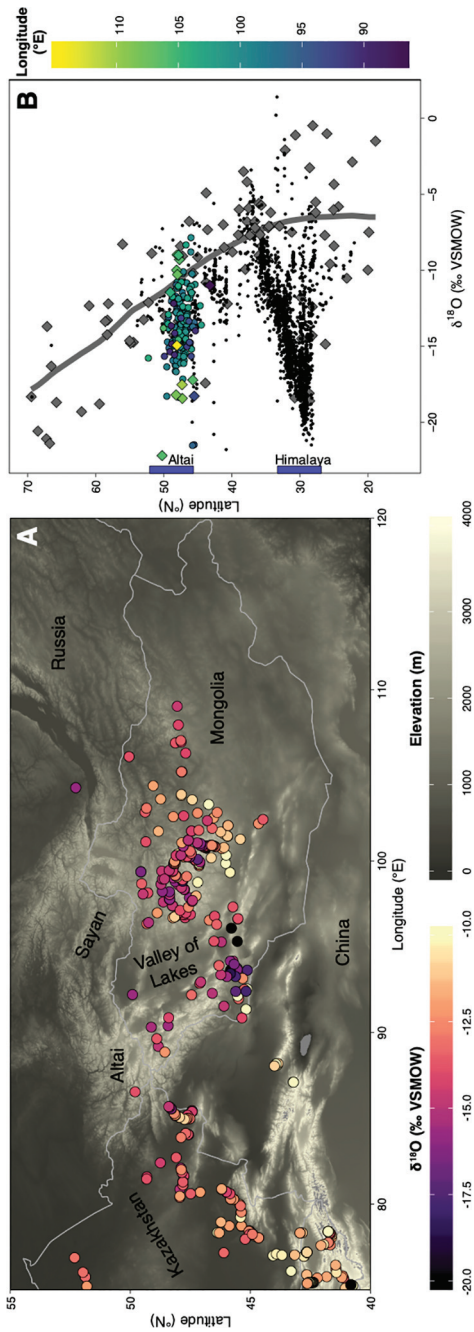

Fig. 3. A) River water $\delta^{18}O$ values in northern central Asia. B) River (circles) and precipitation (diamonds) $\delta^{18}O$ values against latitude. Colored points are from Mongolia; small black points are compiled river water $\delta^{18}O$ data (longitude range: 51°–161°) and gray diamonds are precipitation data (longitude range: 39°–168°) (Sun and others, 2016; Rugenstein and Chamberlain, 2018; Bershaw and Lechler, 2019; Wu and others, 2019; IAEA/WMO, 2020a; IAEA/WMO, 2020b). The solid, gray line is a kernel-smooth average of the latitudinal value of precipitation $\delta^{18}O$, but excluding data from the Tibetan Plateau to better visualize the effect of poleward-rainout—rather than topography—on precipitation $\delta^{18}O$ values. Note the larger latitude range in panel B than in panel A.

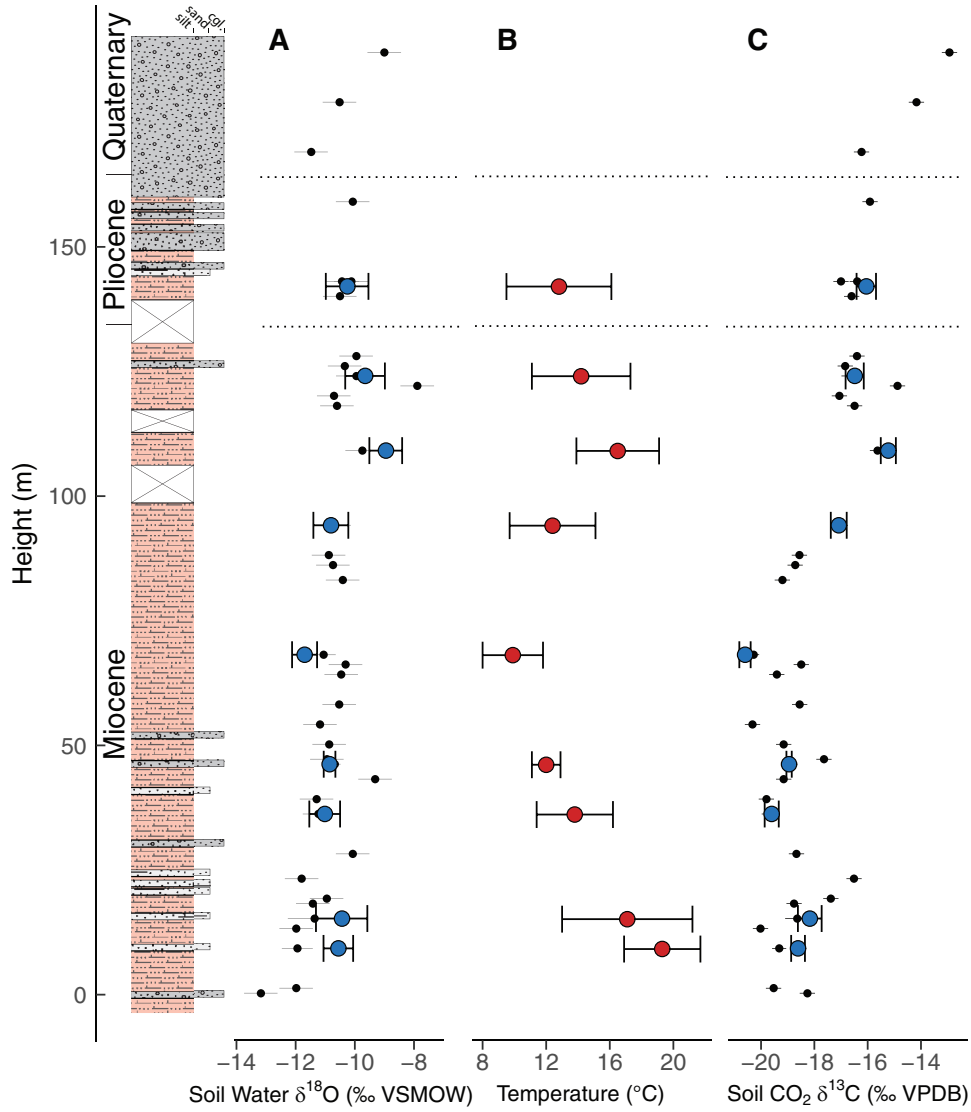

Fig. 4. Reconstructed soil water $\delta^{18}O$ (A) and soil CO_2 $\delta^{13}C$ (C) values based upon measured clumped-isotope temperature data (B) and carbonate $\delta^{18}O$ and $\delta^{13}C$ values. Blue dots in A and C are reconstructed soil water $\delta^{18}O$ and soil CO_2 $\delta^{13}C$ based upon corresponding Δ_{47} data from the same sample; black dots in A and C are reconstructed soil water $\delta^{18}O$ and soil CO_2 $\delta^{13}C$ from soil temperature data interpolated between measured Δ_{47} data. Error bars in B are 1σ and error bars in A and C are propagated ranges in the reconstructed values based upon the 1σ uncertainties in B. Gray error bars on the soil water $\delta^{18}O$ and soil CO_2 $\delta^{13}C$ data are calculated based upon the mean temperature uncertainty (± 1σ) from B.

is a continuous temperature decrease of ~10 °C with the minimum temperature of 9.9 ± 1.9 °C at 68 m. This is followed by an ~7 °C temperature increase from 68 to 109 m, reaching a calculated temperature of 16.5 ± 2.6 °C and by another 4 °C temperature decrease in the upper part of the section (109–142 m), though this last decrease in temperature is within the uncertainty of the temperature estimate.

Assuming isotopic equilibrium during carbonate formation, we use the carbonate formation temperatures to calculate both soil water $\delta^{18}O$ ($\delta^{18}O_{sw}$) using the

fractionation factors of Kim and O'Neil (1997) as well as soil CO_2 $\delta^{13}C$ ($\delta^{13}C_{soil}$) using the fractionation factors compiled in Cerling (1999) (table 2). The reconstructed $\delta^{18}O_{sw}$ values vary between −11.7 and −9‰. Though there is no long-term trend in the lower part of the section, $\delta^{18}O_{sw}$ increases ~2.7‰ coincident with the increase in temperatures. Constant or declining reconstructed $\delta^{13}C_{soil}$ corresponds with decreasing carbonate formation temperature. In contrast, the 7 °C increase in carbonate formation temperature correlates with a large (~5‰) increase in $\delta^{13}C_{soil}$ in the middle of the section (68–109 m) (table 2; fig. 4). In figure 4, to more directly compare with the additional carbonate $\delta^{18}O$ and $\delta^{13}C$ data, we interpolate the temperature data to estimate a carbonate formation temperature for every carbonate stable isotope sample of the Dzereg section and then use these temperatures and the aforementioned fractionation factors to calculate $\delta^{18}O_{sw}$ and $\delta^{13}C_{soil}$ for every sample. For the Quaternary samples, we use the uppermost estimate of temperature (from the Pliocene) as we do not *a priori* know the season of carbonate formation in the Quaternary. As discussed below, the Pliocene temperature estimate suggests that carbonate forms in the early Fall, consistent with the idea that carbonate forms towards the end of the wet season as plants senesce (Breecker and others, 2009; Burgener and others, 2016; Kelson and others, 2020).

DISCUSSION

Both the present-day $\delta^{18}O_{mw}$ data and the HYSPLIT simulations suggest that the presence of the Altai exerts an important influence on lee-side climate. Similarly, geologic data from the lee of the Altai indicate that local climate has changed considerably throughout the late Neogene. Previously, we have shown that uplift of the Altai and Tian Shan in the late Neogene may have altered the seasonality of precipitation on the windward flanks of these ranges (Caves and others, 2017). Below, we discuss how Altai uplift may have changed leeside temperature, precipitation, and plant productivity but maintained constant precipitation $\delta^{18}O$ over the late Neogene despite rising upwind topography.

Interaction of the Altai and Climate

During the first half of every year, the mid-latitude westerly jet migrates northward from south of the Tibetan Plateau in boreal winter to north of the Tibetan Plateau in summer. During this migration, springtime storms that are routed along the jet intersect the high topography of the Tien Shan and Altai, producing orographic precipitation and a peak in rainfall on the windward sides of these ranges (Schiemann and others, 2009; Baldwin and Vecchi, 2016). As seen in HYSPLIT backtrajectories, westerly-originating moisture typically skirts the highest portions of the Altai, resulting in trajectories that veer south or north of the highest peaks (Galewsky, 2009) (fig. 2).

These westerly trajectories result in low $\delta^{18}O_{mw}$ values, particularly in the northern Valley of Lakes, northwest Hangay, and in the western Mongolian Altai, as moisture is distilled on the windward side and low $\delta^{18}O$ moisture is transported eastward (Sato and others, 2007) (fig. 3). All of the samples presented in figure 3A are from rivers and streams, suggesting they may be recording higher-elevation precipitation that feeds the few streams and rivers in western Mongolia. Nevertheless, this potentially high-elevation moisture has substantially lower $\delta^{18}O$ than streams that occur at the same latitude in either central or eastern Mongolia or western Kazakhstan. It is possible that a portion of the spatial pattern of $\delta^{18}O$ is influenced by evaporation, either through sub-cloud evaporation of precipitation (Lee and others, 2012) or surface evaporation, particularly given that the local MWL has a lower slope than the Asia-wide MWL (fig. A1A). However, the slope of the local MWL is not substantially lower than the average local MWL of precipitation globally (Putman and others, 2019),

and there is no obvious longitudinal pattern in the d-excess values (fig. A1B). Consequently, we suggest that these $\delta^{18}O_{mw}$ values record rainout induced by Altai topography upwind of western Mongolia, rather than evaporative effects associated with the arid climate.

Clumped and Stable Isotope Evidence of Past Climate Change

In western Mongolia, $\delta^{13}C_{soil}$ values increase by ~7‰ over the course of the sampled Dzereg basin sedimentary section—one of the largest increases in carbonate or soil CO_2 $\delta^{13}C$ outside of areas impacted by the onset of C4 grass ecosystems in the late Neogene (fig. 4). Even considering only the data constrained by Δ_{47} data, the increase in $\delta^{13}C_{soil}$ is ~5‰. Given that there are few to no C4 grasses in western Mongolia due to the arid and exceptionally cold climate (Still and others, 2003), Caves and others (2014) concluded that this increase in $\delta^{13}C$ reflected a substantial decline in plant productivity. Soil CO_2 $\delta^{13}C$ values represent a balance between atmospheric CO_2, with a $\delta^{13}C$ of ~ −7‰, and soil-respired CO_2 with an average value from C3 root and soil organic matter respiration of ~−25 to −27‰ (Cerling and Quade, 1993; Caves and others, 2016; Licht and others, 2020). Thus, a large increase in $\delta^{13}C_{soil}$ at Dzereg coincident with a large decline in atmospheric pCO_2 during the late Neogene (Herbert and others, 2016; Mejía and others, 2017)—that would tend to lower $\delta^{13}C_{soil}$ all else being equal—suggests an exceptionally large decrease in plant productivity in western Mongolia.

Over the same section, our clumped isotope data suggest that soil temperatures also fell by 6.5 ± 5.7 °C during the Miocene, before increasing and then decreasing into the Pliocene (fig. 4). Though we lack a precise chronology for this section, the relatively low sedimentation rates (Traynor and Sladen, 1995) and modern-day erosion rates (Smith and others, 2016) suggest that the Miocene unit may span much of the epoch. If so, then the overall cooling trend may reflect long-term global cooling during the Neogene, which is particularly pronounced in the Northern Hemisphere after the Middle Miocene Climatic Optimum (Herbert and others, 2016). Soil temperature shifts of this magnitude have been observed in multiple Neogene records (Löffler and others, 2019; Methner and others, 2020) as well as Cenozoic Asian records (Ingalls and others, 2018; Page and others, 2019). Indeed, deeply continental settings such as western Mongolia are thought to be most sensitive to changes in global climate (Kirtman and others, 2013), suggesting that the cooling in western Mongolia over the Neogene may be greater than the change in the global mean surface temperature.

However, a long-term global cooling trend does not reconcile the punctuated increase in Δ_{47}-derived temperatures (6.6 ± 4.5 °C) in the upper part of the Dzereg section, nor does it reconcile how $\delta^{18}O_{sw}$ can increase with Altai uplift, rather than decrease as predicted by stable isotope paleoaltimetry theory (Rowley and others, 2001). To address these points, we propose two scenarios that link Altai uplift to warmer soil carbonate formation temperature and higher $\delta^{18}O_{sw}$. Scenario 1 links the establishment of the Altai rainshadow to increasing land surface temperatures and increasing $\delta^{18}O_{sw}$ via evaporative effects. Scenario 2, in contrast, focuses on the effect of an Altai rainshadow on the seasonality of soil carbonate formation and, therefore, the temperature and $\delta^{18}O_{sw}$ that these minerals record. The key distinction between these scenarios is that scenario 1 explains the observed data in terms of changing environmental conditions (temperature and $\delta^{18}O_{sw}$) while scenario 2 implicates changes in the timing of soil carbonate formation. We stress that these scenarios are not mutually exclusive.

Scenario 1: Altai rainshadow effect on environmental conditions.—The punctuated increase in carbonate formation temperature in the upper part of the Dzereg section,

coincident with increasing $\delta^{13}C_{soil}$ and $\delta^{18}O_{sw}$, can be explained by uplift if the establishment of a rainshadow decreased plant transpiration while increasing the fraction of evaporated water. For example, we previously attributed the increase in $\delta^{13}C_{soil}$ to decreased plant productivity (Caves and others, 2014; Caves and others, 2016). Along with decreased precipitation due to Altai uplift, this decrease in productivity would likely be accompanied by less total biomass and leaf area (Gholz, 1982), decreasing total plant transpiration. Since transpiration works as an "evaporative cooler" by transferring the energy from sunlight into latent heat, thus depressing temperatures relative to a plant-free landscape (Kleidon and others, 2000), decreased transpiration with rainshadow establishment could cause warming (Kelson and others, 2020). Such a reduction in evaporative cooling could be due to Altai surface uplift—and the formation of the Altai rain shadow—or declining atmospheric pCO_2 and global cooling, which may have reduced precipitation and limited plant productivity in western Mongolia (Caves and others, 2016).

Aridification may have also increased the fraction of evaporated water, thereby increasing $\delta^{18}O_{sw}$. Today, the leeward side of the Altai is characterized by lower precipitation and relative humidity compared to the windward side—conditions that are generally associated with increases in raindrop re-evaporation or the evaporative fraction of soil water (Dansgaard, 1964; Blisniuk and Stern, 2005; Bershaw and others, 2012; Lee and others, 2012). If Altai uplift occurred in the late Miocene, the establishment of a rain shadow would have decreased precipitation and relative humidity, increasing the evaporative enrichment of ^{18}O in rainfall and soil water. An evaporatively driven increase in precipitation and soil water $\delta^{18}O$ may have hidden the effect of lower precipitation $\delta^{18}O$ due to increased summertime rainout on the windward side of the Altai. This decrease in relative humidity may have been exacerbated by the rapid decline of vegetation biomass, which would have reduced both transpiration rates—and consequently the re-supply of moisture to the atmosphere—and shade, potentially increasing direct soil evaporation.

Scenario 2: Altai rainshadow effect on soil carbonate formation seasonality.—Alternatively, the observed increase in soil temperature and $\delta^{18}O_{sw}$ may be due to a change in the seasonality of carbonate formation during growth of Altai topography. The youngest clumped isotope data (from the Pliocene unit) yield temperatures and $\delta^{18}O_{mw}$ similar to early- or late-summer (May or September) conditions today (fig. 5). These results are consistent with the finding that carbonates often form as soils dry and plants senesce at the end of the rainy season (Breecker and others, 2009), JJA in Mongolia (fig. 1C). Though several factors can modify precisely when carbonate forms and how temperature and meteoric water $\delta^{18}O$ are recorded in soil carbonates (Huth and others, 2019; Kelson and others, 2020), we suspect that in western Mongolia soil carbonate formation is likely occurring in late summer and early fall, if conditions today are similar to those in the Pliocene.

Given the dependence of soil carbonate formation on the timing of the wet season, if uplift caused a change in precipitation seasonality, it may also drive changes in the timing of soil carbonate formation. Today, the Tien Shan and Altai demarcate a sharp boundary between a spring- and fall-dominated precipitation regime on their windward flanks and a leeward summer-dominated regime (fig. 1C) (Schiemann and others, 2009; Rugenstein and Chamberlain, 2018; Bershaw and Lechler, 2019). Caves and others (2017) found that this boundary likely formed starting in the late Miocene and attributed it to surface uplift of the Altai and Tien Shan. It is conceivable that, before this time, no sharp boundary existed and, instead, western Mongolia received a greater fraction of moisture in spring and fall while also receiving some precipitation in the summer (as observed on the windward flanks of the Altai). Uplift of the Altai may have cut-off spring and fall moisture—through orographic precipitation on the

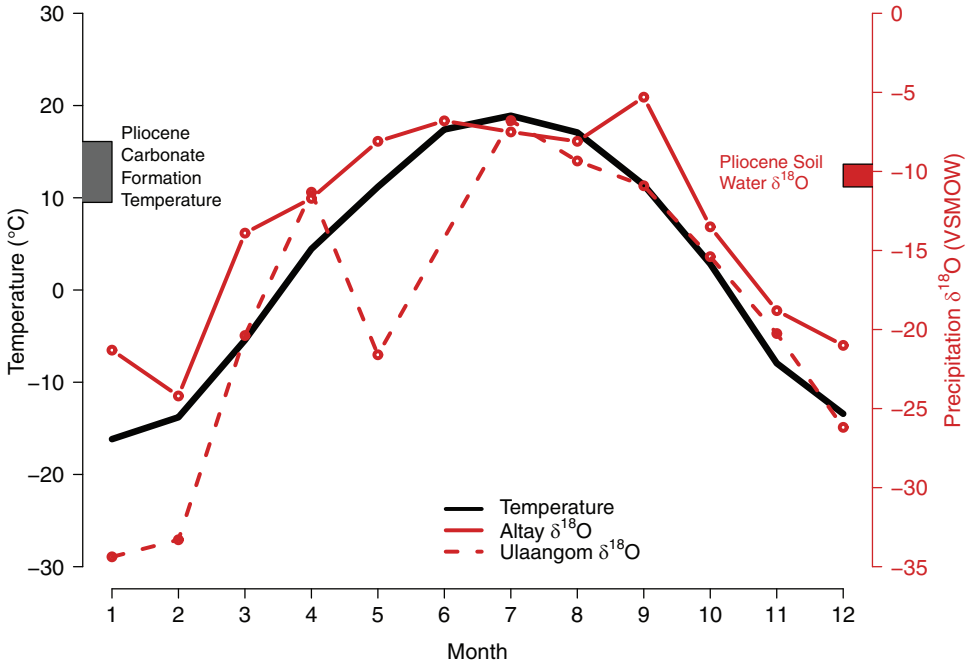

Fig. 5. Comparing modern temperature and precipitation $\delta^{18}O$ data in western Mongolia/northwestern China and reconstructed Pliocene carbonate formation temperature and soil water $\delta^{18}O$. The solid black line is the mean monthly temperature at the Dzereg site, interpolated from 0.5° x 0.5° modern climate output from the NW Climate Toolbox (Hegewisch and Abatzoglou, 2021). The solid red line is precipitation $\delta^{18}O$ from Altay, China (Tian and others, 2007); the dashed red line is precipitation $\delta^{18}O$ from Ulaangom, Mongolia (Kurita and Ichiyanagi, 2008) (note that no data is available for June). The gray box along the left-hand y-axis is the full range (± 1σ) of the estimated formation temperature of Pliocene carbonates; the red box along the right-hand y-axis is the full range (± 1σ) of the estimated Pliocene $\delta^{18}O_{sw}$.

windward flanks—resulting in a greater fraction of precipitation falling in the summer in western Mongolia. This shift in rainfall seasonality—combined with a decrease in total annual precipitation due to the establishment of the Altai rain shadow—may have resulted in a change in the season of soil carbonate formation, from dominantly spring and fall to end-of-summer as observed today. This shift would drive increasing carbonate formation temperatures and increase $\delta^{18}O_{sw}$ as a greater fraction of high ^{18}O summertime precipitation is recorded in soil carbonates (fig. 5). A shift toward more summertime and less spring and fall moisture could potentially increase precipitation $\delta^{18}O$ by ~5‰ assuming a similar-to-modern annual cycle in $\delta^{18}O_{mw}$ (fig. 5), dampening any decrease in $\delta^{18}O_{mw}$ due to uplift. Similarly, soil temperatures would increase, though estimating by how much is hindered by poor constraints on the depth of soil carbonate formation in these samples, which would impact how surface temperature changes are translated down in the soil column (Kelson and others, 2020). Synchronously, $\delta^{13}C_{soil}$ would increase as the overall landscape became drier due to the overall decrease in precipitation.

Possibility of late Miocene climate change without Altai uplift.—Lastly, we cannot rule out that the bulk of Altai uplift occurred before the Miocene—given the extensive Oligocene sedimentary cover and AFT data indicative of enhanced Paleogene exhumation—such that the $\delta^{18}O_{sw}$ signal we observe at Dzereg has already incorporated the primary effects of uplift and windward distillation. If so, the large increase in $\delta^{13}C_{soil}$ and changes in carbonate formation temperatures would be due solely to

global cooling during the Neogene. However, we view this scenario as unlikely given that older carbonate $\delta^{18}O$ records in Mongolia from further east show no large, earlier decrease in carbonate $\delta^{18}O$ (Caves and others, 2014). Additionally, sites further east and south in Asia that are affected by westerly moisture—that would be blocked by Altai uplift—similarly show no signs of a decrease in carbonate $\delta^{18}O$ older than the Miocene and, in fact, typically increase throughout the late Paleogene and Neogene (Caves and others, 2015).

Drivers of Regional Climate Change in Western Mongolia

The stable and clumped isotope data from Dzereg do not uniquely identify which scenario presented above drove the changes we observe nor whether Altai uplift or global cooling was the driver of late Neogene climatic changes in western Mongolia. However, in combination with regional paleoenvironmental records (Czyzewski, 1969; Caves and others, 2014, 2017), they suggest that accelerated Altai uplift in the late Neogene (Frankel and others, 2010)—rather than global cooling alone—shifted the seasonality of precipitation, resulting in the changes we observe in western Mongolia. We summarize that evidence here. To compare our stable isotope data from Dzereg with regional records, we construct a coarse age model, assuming that the decline in temperature begins towards the end of the Middle Miocene Climatic Optimum (MMCO) and following evidence that temperatures in the Northern Hemisphere declined synchronously following the MMCO (Herbert and others, 2016; Methner and others, 2020). For each epoch, we then assume constant sedimentation rates. However, to emphasize the uncertainty in our age model, we also average the data by epoch in order to limit our conclusions to the resolution of the biostratigraphy available at Dzereg (fig. 6) (Gradzinski and others, 1969) (we do not average the Δ_{47} data by epoch because we only have one datapoint outside the Miocene). We note that this age model differs from that previously presented in Caves and others (2014), which assumed that nearly the entire Miocene epoch was represented in the Dzereg basin.

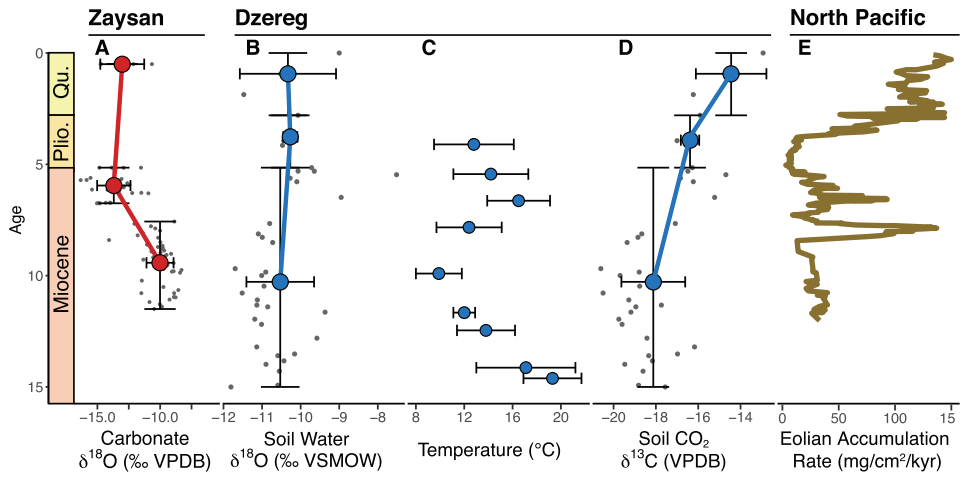

Fig. 6. A comparison of regional climate change data during the late Neogene. Here, stable isotope data from Dzereg has been assigned to an age model (gray points), but the stable isotope data has also been averaged by epoch (large, colored points). A) Carbonate $\delta^{18}O$ data from Zaysan. B) Soil water $\delta^{18}O$ data from Dzereg. C) Clumped isotope-based carbonate formation temperatures from Dzereg. D) Soil CO_2 $\delta^{13}C$ from Dzereg. E) Eolian accumulation rate of dust in the North Pacific (replotted from Rea and others, 1998). In A, B, and D, horizontal error bars are 1σ. of the averaged data; vertical error bars are a range of possible ages as constrained by biostratigraphy. In C, horizontal error bars are 1σ of the Δ_{47} data.

Given that soil temperatures decline substantially at Dzereg, we suggest that this is likely to track cooling during the late Neogene; however, we stress that this age model remains uncertain and requires further refinement. Nevertheless, as outlined below, with these assumptions, the increase in soil temperatures and $\delta^{13}C_{soil}$ is broadly coincident with regional changes that may share the same mechanism—uplift of the Altai.

First, the increase in temperature and in $\delta^{13}C_{soil}$ values is approximately coincident with a sharp decline in paleosol carbonate $\delta^{18}O$ values from the Zaysan basin (Caves and others, 2017), located windward of the Altai (fig. 6). Caves and others (2017) attributed this decrease in carbonate $\delta^{18}O$ to a shift towards spring and fall precipitation and away from summertime precipitation due to uplift of the Altai and Tien Shan and enhanced interaction of the mid-latitude westerly jet with this high topography. Purely an increase in arid, evaporative conditions in the Altai lee following uplift (Scenario 1) would not likely result in a synchronous shift in windward $\delta^{18}O$, suggesting that Scenario 2 is more likely. Second, the increase in soil temperature and in $\delta^{13}C_{soil}$ and $\delta^{18}O_{sw}$ at Dzereg also approximately correlates with a substantial increase in dust deposition in the Late Miocene in the North Pacific (fig. 6) (Rea and others, 1998). Today, dust is transported to the North Pacific by the lee cyclones that develop in the lee of the Altai (Shao and Dong, 2006; Roe, 2009). The increase in eolian accumulation rate in the North Pacific during the late Miocene-Pliocene suggests that Altai topography was high enough by the late Neogene to generate increasingly windy conditions conducive to large-scale dust transport. The development of dust-generating conditions may have been further aided by the large-scale collapse of plant productivity due to the simultaneous establishment of the Altai rain shadow and potential positive feedbacks between dust generation and surface albedo (Abell and others, 2020). Indeed, the increase in $\delta^{13}C$ is the largest increase in soil CO_2 or carbonate $\delta^{13}C$ documented in Asia outside of areas impacted by C4 vegetation in the late Neogene (Quade and others, 1989; Caves and others, 2016). Though $\delta^{13}C$ increases everywhere in Asia during the Neogene, suggesting a long-term continent-wide decline in plant productivity (Caves and others, 2016; Rugenstein and Chamberlain, 2018), the exceptionally large increase at Dzereg indicates that another factor—likely Altai uplift—additionally depressed plant productivity in addition to what global cooling and declining atmospheric pCO_2 would do.

The above scenario—uplift-driven shift in precipitation seasonality—is one plausible link between Altai uplift and the subsequent climatic response that connects several regional paleoclimate records. Further, late Neogene uplift of the Altai may explain many concomitant changes in climate that occurred across Asia—such as increased Loess Plateau deposition rates (Molnar and others, 2010) and enhanced aridification within the deserts of China (Sun and others, 2015)—given the pronounced impact of the Altai on regional climate.

Decoupling of Uplift and Climate Change

Our stable and clumped isotope data point towards Altai uplift as the most likely driver of the substantial climatic changes in the lee of the Altai during the Neogene. However, sedimentation beginning in the late Eocene and Oligocene in the Valley of Lakes indicates an earlier onset of uplift (Traynor and Sladen, 1995; Cunningham and others, 1996; Cunningham, 1998; Howard and others, 2003). Further, some thermochronological data show enhanced exhumation starting in the late Oligocene and early Miocene (Yuan and others, 2006; Glorie and others, 2012), well before the observed shifts in climate in the late Neogene. We speculate that these divergent dates of uplift between the paleoclimate proxies and the sedimentary and thermochronological data are not inconsistent; rather, they suggest that, while Altai uplift started in the Oligocene—similar to estimates of renewed uplift in the Tien Shan (Hendrix and

others, 1994)—surface topography did not approach elevations high enough to modify local climate substantially until the late Miocene.

Such temporal decoupling of the onset of Altai uplift and the observed climatic changes in the lee of the Altai may arise from several mechanisms. First, as climate cooled during the Neogene, the climatological position of the westerly jet that steers storms towards the Altai and Tien Shan may have shifted southward (Shaw and others, 2016; Abell and others, 2021), increasing the interaction of the jet and high topography. Second, the large shifts in climate observed in both western Mongolia and eastern Kazakhstan occur during the late Miocene—a period of major Northern Hemisphere cooling (Herbert and others, 2016)—suggesting that a southward shift in the jet may have wrought these changes as it increasingly interacted with the high topography of the Tien Shan and Altai. Alternatively, the thin Cenozoic sediments in the closed Valley of Lakes suggest that uplift rates have been relatively slow; erosion rates from the nearby Hangay Mountains are also lower than expected, despite the high elevation and local relief (Smith and others, 2016). Consequently, while exhumation may have initiated in the late Paleogene, the relatively slow uplift rates may not have elevated topography sufficiently to interact with the westerly jet until the late Miocene. Given the extreme continentality of the Altai—and hence low moisture content of the atmosphere in this part of Asia—it is possible that orographic rainout only occurs once topography is high enough to force sufficient lifting of air parcels to form precipitation. Testing this decoupling and these hypothesized mechanisms will require additional work to constrain the timing of exhumation and regional climate change as well as modeling to test how exceptionally continental ranges affect climate.

CONCLUSIONS

Though much work on paleoclimate in Asia focuses on the Tibetan Plateau's role in modifying climate, the ranges to the north—particularly the Altai Mountains—profoundly influence Asia's climate today. We provide new data from the immediate lee of the Altai to analyze how climate has changed during the late Miocene and assess how Altai uplift might have influenced climate in western Mongolia. Today, the Altai cast a considerable rain shadow, shunting storms around the bulk of high topography and leading to lower $\delta^{18}O_{mw}$ values in the immediate lee of the Altai. Although we observe an overall decrease in lee-side soil temperatures, the Dzereg Δ_{47} soil carbonate record is punctuated by an increase in soil temperature that corresponds with the largest increase in $\delta^{13}C_{soil}$ values in the Dzereg sedimentary section, which reflects a decline in plant productivity, and with a small increase in reconstructed $\delta^{18}O_{sw}$. We suggest that this coincident increase in $\delta^{13}C_{soil}$ and soil temperature reflects aridification due to the establishment of the Altai rain shadow and a reduction in transpiration rates, which would have increased soil temperatures by partitioning a greater amount of the incoming radiative energy to ground heating, rather than to evaporation of water, particularly as plant productivity and leaf area decreased. Paradoxically, reconstructed $\delta^{18}O_{sw}$ does not decrease synchronously, as stable isotopic paleoaltimetry would predict, and instead increases or remains constant as soil temperatures increase. Given the synchronous decrease in $\delta^{18}O$ observed in the Zaysan Basin windward of the Altai, we instead suggest that Altai uplift shifted precipitation seasonality towards summer, thereby offsetting any decrease in precipitation $\delta^{18}O$ due to uplift and windward moisture distillation.

These late Neogene changes in western Mongolia are approximately synchronous with a host of climatic changes throughout Asia that may be attributable to Altai uplift. Altai uplift seemingly shifted the seasonal distribution of moisture in Asia, as reflected by declining paleosol carbonate $\delta^{18}O$ values in windward basins and increasing $\delta^{18}O$

in leeward basins. In addition, Altai uplift may have further increased dustiness across Asia due to an increase in lee cyclogenesis (Roe, 2009). Though several records of exhumation from the Altai—including AFT data and sedimentation rates—indicate that Altai uplift in the Cenozoic initiated in the late Paleogene, we suggest that the disconnect between these exhumation records and records of climate in western Mongolia may reflect a delay between when exhumation resumed in the Cenozoic and when the Altai achieved elevations high enough to influence climate. Collectively, these records suggest that the uplift of the Altai—along with the other high ranges north of the Plateau—may be critical to understanding long-term climate change in Asia in the late Neogene.

ACKNOWLEDGMENTS

We thank the many laboratory managers and technicians who helped acquire data for this project, including Ulrich Treffert, Sven Hofman, and Daniel Montluçon. We also thank Miquela Ingalls and two anonymous reviewers who provided valuable critiques of this manuscript. An Alexander von Humboldt Postdoctoral Fellowship partly funded JKCR, and funding for fieldwork was provided by NSF grant EAR-1009721 to CPC.

SUPPLEMENTARY TABLES

http://earth.eps.yale.edu/%7eajs/SupplementaryData/2022/Rugenstein

APPENDIX

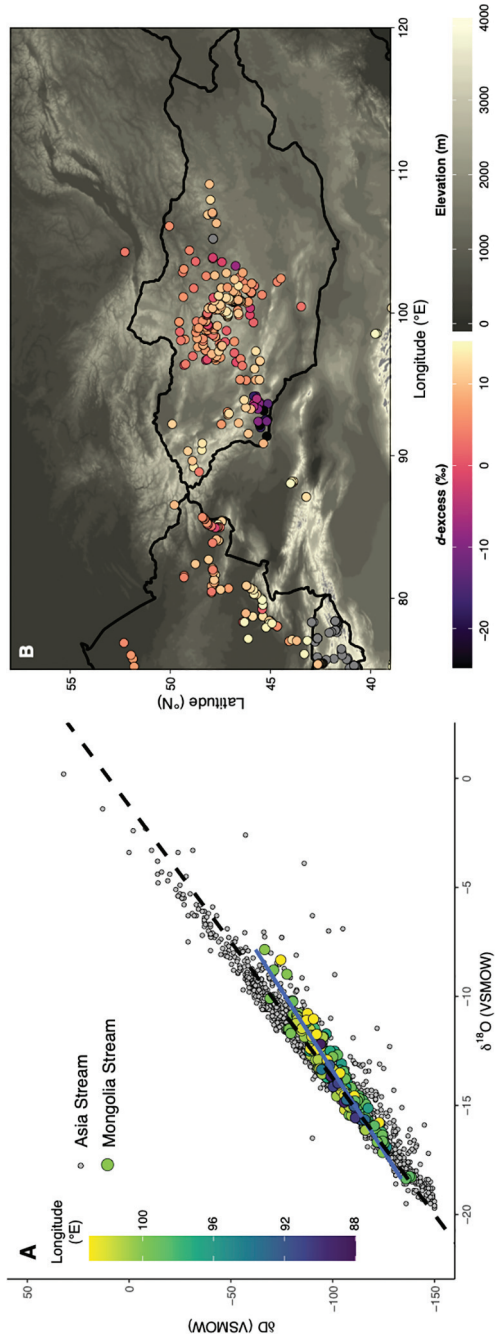

Fig. A1. (A) Plot of the meteoric water line in Asia (dashed line with gray points indicating individual stream data) and in Mongolia (blue line with points colored by longitude). (B) Map of *d*-excess (‰) in Mongolia. Gray points are previously published data for which δD was not available. The cluster of low *d*-excess points in southwest Mongolia are from a wetland ecosystem, reported by Burnik Sturm (2017).

REFERENCES

Abell, J. T., Pullen, A., Lebo, Z. J., Kapp, P., Gloege, L., Metcalf, A. R., Nie, J., and Winckler, G., 2020, A wind-albedo-wind feedback driven by landscape evolution: Nature communications, v. 11, 96, https://doi.org/10.1038/s41467-019-13661-w

Abell, J. T., Winckler, G., Anderson, R. F., and Herbert, T. D., 2021, Poleward and weakened westerlies during Pliocene warmth: Nature, v. 589, p. 70–75, https://doi.org/10.1038/s41586-020-03062-1

Aizen, E. M., Aizen, V. B., Melack, J. M., Nakamura, T., and Ohta, T., 2001, Precipitation and atmospheric circulation patterns at mid-latitudes of Asia: International Journal of Climatology, v. 21, n. 5, p. 535–556, https://doi.org/10.1002/joc.626

An, Z., Kutzbach, J. E., Prell, W. L., and Porter, S. C., 2001, Evolution of Asian monsoons and phased uplift of the Himalaya-Tibetan plateau since Late Miocene times: Nature, v. 411, p. 62–66, https://doi.org/10.1038/35075035

Bajnai, D., Fiebig, J., Tomašových, A., Milner Garcia, S., Rollion-Bard, C., Raddatz, J., Löffler, N., Primo-Ramos, C., and Brand, U., 2018, Assessing kinetic fractionation in brachiopod calcite using clumped isotopes: Scientific Reports, v. 8, 533, https://doi.org/10.1038/s41598-017-17353-7

Baldwin, J., and Vecchi, G., 2016, Influence of the Tian Shan Mountains on Arid Extratropical Asia: Journal of Climate, v. 29, p. 5741–5762, https://doi.org/10.1175/JCLI-D-15-0490.1

Bershaw, J., and Lechler, A. R., 2019, The isotopic composition of meteoric water along altitudinal transects in the Tian Shan of Central Asia: Chemical Geology, v. 516, p. 68–78, https://doi.org/10.1016/j.chemgeo.2019.03.032

Bershaw, J., Penny, S. M., and Garzione, C. N., 2012, Stable isotopes of modern water across the Himalaya and eastern Tibetan Plateau: Implications for estimates of paleoelevation and paleoclimate: Journal of Geophysical ResearchL: Atmospheres, v. 117, n. D2, D02110, https://doi.org/10.1029/2011JD016132

Blisniuk, P. M., and Stern, L. A., 2005, Stable Isotope Paleoaltimetry: A critical review: American Journal of Science, v. 305, n. 10, p. 1033–1074, https://doi.org/10.2475/ajs.305.10.1033

Botsyun, S., Sepulchre, P., Donnadieu, Y., Risi, C., Licht, A., and Caves Rugenstein, J. K., 2019, Revised paleoaltimetry data show low Tibetan Plateau elevation during the Eocene: Science, v. 363, n. 6430, eaaq1436, https://doi.org/10.1126/science.aaq1436

Breecker, D. O., Sharp, Z. D., and McFadden, L. D., 2009, Seasonal bias in the formation and stable isotopic composition of pedogenic carbonate in modern soils from central New Mexico, USA: Geological Society of America Bulletin, v. 121, n. 3–4, p. 630–640, https://doi.org/10.1130/B26413.1

Burgener, L., Huntington, K. W., Hoke, G. D., Schauer, A., Ringham, M. C., Latorre, C., and Díaz, F. P., 2016, Variations in soil carbonate formation and seasonal bias over >4 km of relief in the western Andes (30°S) revealed by clumped isotope thermometry: Earth and Planetary Science Letters, v. 441, p. 188–199, https://doi.org/10.1016/j.epsl.2016.02.033

Burnik Šturm, M., Ganbaatar, O., Voigt, C. C., and Kaczensky, P., 2017, First field-based observations of δ^2H and $\delta^{18}O$ values of event-based precipitation, rivers and other water bodies in the Dzungarian Gobi, SW Mongolia: Isotopes in Environmental and Health Studies, v. 53, p. 157–171, https://doi.org/10.1080/10256016.2016.1231184

Caves, J. K., Sjostrom, D. J., Mix, H. T., Winnick, M. J., and Chamberlain, C. P., 2014, Aridification of Central Asia and Uplift of the Altai and Hangay Mountains, Mongolia: Stable Isotope Evidence: American Journal of Science, v. 314, n. 8, p. 1171–1201, https://doi.org/10.2475/08.2014.01

Caves, J. K., Winnick, M. J., Graham, S. A., Sjostrom, D. J., Mulch, A., and Chamberlain, C. P., 2015, Role of the westerlies in Central Asia climate over the Cenozoic: Earth and Planetary Science Letters, v. 428, p. 33–43, https://doi.org/10.1016/j.epsl.2015.07.023

Caves, J. K., Moragne, D. Y., Ibarra, D. E., Bayshashov, B. U., Gao, Y., Jones, M. M., Zhamangara, A., Arzhannikova, A. V., Arzhannikov, S. G., and Chamberlain, C. P., 2016, The Neogene de-greening of Central Asia: Geology, v. 44, n. 11, p. 887–890, https://doi.org/10.1130/G38267.1

Caves, J. K., Bayshashov, B. U., Zhamangara, A., Ritch, A. J., Ibarra, D. E., Sjostrom, D. J., Mix, H. T., Winnick, M. J., and Chamberlain, C. P., 2017, Late Miocene uplift of the Tian Shan and Altai and reorganization of Central Asia climate: GSA Today, v. 27, n. 2, p. 19–26, https://doi.org/10.1130/GSATG305A.1

Cerling, T. E., 1999, Stable carbon isotopes in palaeosol carbonates, *in* Thiry, M., and Simon-Coinçon, R. editors., Palaeoweathering, Palaeosurfaces and Related Continental Deposits: The International Association of Sedimentologists, p. 43–60, https://doi.org/10.1002/9781444304190.ch2

Cerling, T. E., and Quade, J., 1993, Stable Carbon and Oxygen Isotopes in Soil Carbonates, *in* Swart, P., Lohmann, K. C., McKenzie, J., and Savin, S. editors., Climate Change in Continental Isotopic Records: Geophysical Monograph Series, American Geophysical Union, Washington, DC, p. 217–231, https://doi.org/10.1029/GM078p0217

Chen, S., and Lazic, L., 1990, Numerical Case Study of the Altai-Sayan Lee Cyclogenesis over East Asia: Meteorology and Atmospheric Physics, v. 42, p. 221–229, https://doi.org/10.1007/BF01314826

Creamean, J. M., Suski, K. J., Rosenfeld, D., Cazorla, A., Demott, P. J., Sullivan, R. C., White, A. B., Ralph, F. M., Minnis, P., Comstock, J. M., Tomlinson, J. M., and Prather, K. A., 2013, Dust and Biological Aerosols from the Sahara and Asia Influence Precipitation in the Western U.S.: Science, v. 339, n. 6127, p. 1572–1578, https://doi.org/10.1126/science.1227279

Cunningham, W. D., 1998, Lithospheric controls on late Cenozoic construction of the Mongolian Altai: Tectonics, v. 17, n. 6, p. 891–902, https://doi.org/10.1029/1998TC900001

Cunningham, W. D., Windley, B. F., Dorjnamjaa, D., Badamgarov, G., and Saandar, M., 1996, A structural transect across the Mongolian Western Altai: Active transpressional mountain building in central Asia: Tectonics, v. 15, n. 1, p. 142–156, https://doi.org/10.1029/95TC02354

Czyzewski, T., 1969, Remains of the Lower Pliocene Bovidae from Altan Teli, Western Mongolia: Palaeontologia Polonica, v. 21, p. 95–104.
Daëron, M., Blamart, D., Peral, M., and Affek, H. P., 2016, Absolute isotopic abundance ratios and the accuracy of Δ_{47} measurements: Chemical Geology, v. 442, p. 83–96, https://doi.org/10.1016/j.chemgeo.2016.08.014
Dansgaard, W., 1964, Stable isotopes in precipitation: Tellus, v. 16, n.4, p. 436–468, https://doi.org/10.3402/tellusa.v16i4.8993
De Grave, J., De Pelsmaeker, E., Zhimulev, F. I., Glorie, S., Buslov, M. M., and Van den Haute, P., 2014, Meso-Cenozoic building of the northern Central Asian Orogenic Belt: Thermotectonic history of the Tuva region: Tectonophysics, v. 621, p. 44–59, https://doi.org/10.1016/j.tecto.2014.01.039
Dennis, K. J., Affek, H. P., Passey, B. H., Schrag, D. P., and Eiler, J. M., 2011, Defining an absolute reference frame for "clumped" isotope studies of CO_2: Geochimica et Cosmochimica Acta, v. 75, n. 22, p. 7117–7131, https://doi.org/10.1016/j.gca.2011.09.025
Devyatkin, E. V, 1981, The Cenozoic of Inner Asia: Stratigraphy, geochronology and correlation: The Joint Soviet-Mongolian Scientific-Research Geological Expedition, Transactions, v. 27, p. 1–196.
Draxler, R. R., and Hess, G., 1998, An Overview of the HYSPLIT_4 Modelling System for Trajectories, Dispersion, and Deposition: Australian Meteorological Magazine, v. 47, p. 295–308.
Fiebig, J., Hofmann, S., Löffler, N., Lüdecke, T., Methner, K., and Wacker, U., 2016, Slight pressure imbalances can affect accuracy and precision of dual inlet-based clumped isotope analysis: Isotopes in Environmental and Health Studies, v. 52, n. 1–2, p. 12–28, https://doi.org/10.1080/10256016.2015.1010531
Fiebig, J., Bajnai, D., Löffler, N., Methner, K., Krsnik, E., Mulch, A., and Hofmann, S., 2019, Combined high-precision Δ_{48} and Δ_{47} analysis of carbonates: Chemical Geology, v. 522, p. 186–191, https://doi.org/10.1016/j.chemgeo.2019.05.019
Frankel, K. L., Wegmann, K. W., Bayasgalan, A., Carson, R. J., Bader, N. E., Adiya, T., Bolor, E., Durfey, C. C., Otgonkhuu, J., Sprajcar, J., Sweeney, K. E., Walker, R. T., Marstellar, T. L., and Gregory, L., 2010, Late Pleistocene slip rate of the Hõh Serh-Tsagaan Salaa fault system, Mongolian Altai and intracontinental deformation in central Asia: Geophysical Journal International, v. 183, n. 3, p. 1134–1150, https://doi.org/10.1111/j.1365-246X.2010.04826.x
Galewsky, J., 2009, Orographic precipitation isotopic ratios in stratified atmospheric flows: Implications for paleoelevation studies: Geology, v. 37, n. 9, p. 791–794, https://doi.org/10.1130/G30008A.1
Garzione, C. N., Dettman, D. L., Quade, J., DeCelles, P. G., and Butler, R. F., 2000, High times on the Tibetan Plateau: Paleoelevation of the Thakkhola graben, Nepal: Geology, v. 28, n. 4, p. 339–342, https://doi.org/10.1130/0091-7613(2000)028<0339:HTOTTP>2.3.CO;2
Gholz, H. L., 1982, Environmental limits on aboveground net primary production, leaf area, and biomass in vegetation zones of the Pacific Northwest: Ecology, v. 63, n. 2, p. 469–481, https://doi.org/10.2307/1938964
Glorie, S., and De Grave, J., 2016, Exhuming the Meso-Cenozoic Kyrgyz Tianshan and Siberian Altai-Sayan: A review based on low-temperature thermochronology: Geoscience Frontiers, v. 7, n. 2, p. 155–170, https://doi.org/10.1016/j.gsf.2015.04.003
Glorie, S., De Grave, J., Buslov, M. M., Zhimulev, F. I., Elburg, M. A., and Van den haute, P., 2012, Structural control on Meso-Cenozoic tectonic reactivation and denudation in the Siberian Altai: Insights from multi-method thermochronometry: Tectonophysics, v. 544–545, p. 75–92, https://doi.org/10.1016/j.tecto.2012.03.035
Gradzinski, R., Kazmierczak, J., and Lefeld, J., 1969, Geographical and geological data from the Polish-Mongolian Palaeontological Expeditions: Palaeontologia Polonica, v. 19, p. 33–82.
Gregory, L. C., Mac Niocaill, C., Walker, R. T., Bayasgalan, G., and Craig, T. J., 2018, Vertical axis rotation (or lack thereof) of the eastern Mongolian Altay Mountains: Implications for far-field transpressional mountain building: Tectonophysics, v. 736, p. 31–46, https://doi.org/10.1016/j.tecto.2018.03.020
Hahn, D. G., and Manabe, S., 1975, The Role of Mountains in the South Asian Monsoon Circulation: Journal of the Atmospheric Sciences, v. 32, n. 8, p. 1515–1541, https://doi.org/10.1175/1520-0469(1975)032<1515:TROMIT>2.0.CO;2
Hegewisch, K. C., and Abatzoglou, J. T., 2021, Historical Climograph web tool, Climate Toolbox, https://climatetoolbox.org/tool/Historical-Climograph
Hendrix, M., Dumitru, T., and Graham, S., 1994, Late Oligocene-early Miocene unroofing in the Chinese Tian Shan: An early effect of the India-Asia collision: Geology, v. 22, n. 6, p. 487–490, https://doi.org/10.1130/0091-7613(1994)022<0487:LOEMUI>2.3.CO;2
Herbert, T. D., Lawrence, K. T., Tzanova, A., Peterson, L. C., Caballero-Gill, R., and Kelly, C. S., 2016, Late Miocene global cooling and the rise of modern ecosystems: Nature Geoscience, v. 9, p. 843–847, https://doi.org/10.1038/ngeo2813
Howard, J. P., Cunningham, W. D., Davies, S. J., Dijkstra, A. H., and Badarch, G., 2003, The stratigraphic and structural evolution of the Dzereg Basin, western Mongolia: clastic sedimentation, transpressional faulting and basin destruction in an intraplate, intracontinental setting: Basin Research, v. 15, n. 1, p. 45–72, https://doi.org/10.1046/j.1365-2117.2003.00198.x
Huth, T. E., Cerling, T. E., Marchetti, D. W., Bowling, D. R., Ellwein, A. L., and Passey, B. H., 2019, Seasonal Bias in Soil Carbonate Formation and Its Implications for Interpreting High-Resolution Paleoarchives: Evidence From Southern Utah: Journal of Geophysical Research: Biogeosciences, v. 124, n. 3, p. 616–632, https://doi.org/10.1029/2018JG004496
IAEA/WMO, 2020a, Global Network of Isotopes in Precipitation, accessed April 10, 2016, The GNIP Database, http://www.iaea.org/water.
IAEA/WMO, 2020b, Global Network of Isotopes in Rivers, The GNIR Database.

Ingalls, M., Rowley, D., Olack, G., Currie, B., Li, S., Schmidt, J., Tremblay, M., Polissar, P., Shuster, D. L., Lin, D., and Colman, A., 2018, Paleocene to Pliocene; pw-latitude, high elevation of southern Tibet: Implications for tectonic models of India-Asia collision, Cenozoic climate, and geochemical weathering: Geological Society of America Bulletin, v. 130, n. 1–2, p. 307–330, https://doi.org/10.1130/B31723.1

Ingalls, M., Rowley, D. B., Currie, B. S., and Colman, A. S., 2020, Reconsidering the uplift history and peneplanation of the northern Lhasa terrane, Tibet: American Journal of Science, v. 320, n. 6, p. 479–532, https://doi.org/10.2475/06.2020.01

Kanamitsu, M., 1989, Description of the NMC Global Data Assimilation and Forecast System: Weather and Forecasting, v. 4, n. 3, p. 335–342, https://doi.org/10.1175/1520-0434(1989)004<0335:DOTNGD>2.0.CO;2

Kelson, J. R., Huntington, K. W., Breecker, D. O., Burgener, L. K., Gallagher, T. M., Hoke, G. D., and Petersen, S. V., 2020, A proxy for all seasons? A synthesis of clumped isotope data from Holocene soil carbonates: Quaternary Science Reviews, v. 234, 106259, https://doi.org/10.1016/j.quascirev.2020.106259

Kim, S., and O'Neil, J. R., 1997, Equilibrium and nonequilibrium oxygen isotope effects in synthetic carbonates: Geochimica et Cosmochimica Acta, v. 61, n. 16, p. 3461–3475, https://doi.org/10.1016/S0016-7037(97)00169-5

Kirtman, B., Power, S. B., Adedoyin, A. J., Boer, G. J., Bojariu, R., Camilloni, I., Doblas-Reyes, F., Fiore, A. M., Kimoto, M., Meehl, G., Prather, M., Sarr, A., Schär, C., Sutton, R., van Oldenborgh, G. J., Vecchi, G., and Wang, H.-J, 2013, Near-term Climate Change: Projections and Predictability, *in* Stocker, T. F., Qin, D., Plattner, G.-K., Tignor, M., Allen, S. K., Boschung, J., Nauels, A., Xia, Y., Bex, V., and Midgley, P. M., editors., Climate Change 2013: The Physical Science Basis. Contribution of Working Group I to the Fifth Assessment Report of the Intergovernmental Panel on Climate Change: New York, Cambridge University Press, p. 953–1028.

Kleidon, A., Fraedrich, K., and Heimann, M., 2000, A green planet versus a desert world: Estimating the maximum effect of vegetation on the land surface climate: Climatic Change, v. 44, p. 471–493, https://doi.org/10.1023/A:1005559518889

Kukla, T., Winnick, M. J., Maher, K., Ibarra, D. E., and Chamberlain, C. P., 2019, The Sensitivity of Terrestrial $\delta^{18}O$ Gradients to Hydroclimate Evolution: Journal of Geophysical Research: Atmospheres, v. 124, n. 2, p. 563–582, https://doi.org/10.1029/2018JD029571

Kurita, N., and Ichiyanagi, K., 2008, Daily basis precipitation sampling network for water isotope analysis: Institute of Observational Research for Global Change, Japan Agency for Marine-Earth Science and Technology, http://www.jamstec.go.jp/iorgc/hcorp/data

Kutzbach, J. E., Prell, W. L., and Ruddiman, W. F., 1993, Sensitivity of Eurasian Climate to Surface Uplift of the Tibetan Plateau: The Journal of Geology, v. 101, n. 2, p. 177–190, https://doi.org/10.1086/648215

Lechler, A. R., and Galewsky, J., 2013, Refining paleoaltimetry reconstructions of the Sierra Nevada, California, using air parcel trajectories: Geology, v. 41, n. 2, p. 259–262, https://doi.org/10.1130/G33553.1

Lee, J.-E., Risi, C., Fung, I., Worden, J., Scheepmaker, R. A., Lintner, B., and Frankenberg, C., 2012, Asian monsoon hydrometeorology from TES and SCIAMACHY water vapor isotope measurements and LMDZ simulations: Implications for speleothem climate record interpretation: Journal of Geophysical Research: Atmospheres, v. 117, n. D15, D15112, https://doi.org/10.1029/2011JD017133

Licht, A., Dupont-Nivet, G., Meijer, N., Caves Rugenstein, J. K., Schauer, A., Fiebig, J., Mulch, A., Hoorn, C., Barbolini, N., and Guo, Z., 2020, Decline of soil respiration in northeastern Tibet through the transition into the Oligocene icehouse: Palaeogeography, Palaeoclimatology, Palaeoecology, v. 560, 110016, https://doi.org/10.1016/j.palaeo.2020.110016

Löffler, N., Fiebig, J., Krijgsman, W., and Mulch, A., 2019, The Magnitude of Continental Temperature Change during the Middle Miocene Climatic Transition in Southern Europe, American Geophysical Union Fall Meeting Abstracts: p. PP14A-08.

McDannell, K. T., Zeitler, P. K., and Idleman, B. D., 2018, Relict Topography Within the Hangay Mountains in Central Mongolia: Quantifying Long-Term Exhumation and Relief Change in an Old Landscape: Tectonics, v. 37, n. 8, p. 2531–2558, https://doi.org/10.1029/2017TC004682

Mejía, L. M., Méndez-Vicente, A., Abrevaya, L., Lawrence, K., Ladlow, C., Bolton, C., Cacho, I., and Stoll, H., 2017, A diatom record of CO_2 decline since the late Miocene: Earth and Planetary Science Letters, v. 479, p. 18–33, https://doi.org/10.1016/j.epsl.2017.08.034

Meltzer, A., Ancuta, L. D., Carlson, R. W., Caves Rugenstein, J. K., Chamberlain, C. P., Gosse, J. C., Idleman, B. D., Ionov, D. A., McDannell, K. T., Mendelson, T., Mix, H. T., Munkhuu, U., Russo, R.M., Sabaj-Perez, M., Sahagian, D. L., Sjostrom , D. J., Smith, S. G., Stachnik, J. C., Tsagaan, B., Wegmann, K. W., Winnick, M, Zitler, P. K., and Proussevitch, A. A., 2015, Betwixt and Between: Structure and Evolution of Central Mongolia, American Geophysical Union Fall Meeting, p. T22A-05.

Merritt, D. A., and Hayes, J. M., 1994, Factors Controlling Precision and Accuracy in Isotope-Ratio-Monrtoring Mass Spectrometry: Analytical Chemistry, v. 66, n. 14, p. 2336–2347, https://doi.org/10.1021/ac00086a020

Methner, K., Campani, M., Fiebig, J., Löffler, N., Kempf, O., and Mulch, A., 2020, Middle Miocene long-term continental temperature change in and out of pace with marine climate records: Scientific Reports, v. 10, 7989, https://doi.org/10.1038/s41598-020-64743-5

Meyer-Christoffer, A., Becker, A., Finger, P., Rudolf, B., Schneider, U., and Ziese, M., 2015, GPCC Climatology Version 2015 at 0.25°: Monthly Land-Surface Precipitation Climatology for Every Month and the Total Year from Rain-Gauges built on GTS-based and Historic Data: Offenbach, Germany, Global Precipitation Climatology Centre (GPCC).

Molnar, P., Boos, W. R., and Battisti, D. S., 2010, Orographic Controls on Climate and Paleoclimate of Asia: Thermal and Mechanical Roles for the Tibetan Plateau: Annual Review of Earth and Planetary Sciences, v. 38, p. 77–102, https://doi.org/10.1146/annurev-earth-040809-152456

Oster, J. L., Montañez, I. P., and Kelley, N. P., 2012, Response of a modern cave system to large seasonal precipitation variability: Geochimica et Cosmochimica Acta, v. 91, p. 92–108, https://doi.org/10.1016/j.gca.2012.05.027

Page, M., Licht, A., Dupont-Nivet, G., Meijer, N., Barbolini, N., Hoorn, C., Schauer, A., Huntington, K., Bajnai, D., Fiebig, J., Mulch, A., and Guo, Z., 2019, Synchronous cooling and decline in monsoonal rainfall in northeastern Tibet during the fall into the Oligocene icehouse: Geology, v. 47, n. 3, p. 203–206, https://doi.org/10.1130/G45480.1

Penny, S., Roe, G. H., and Battisti, D. S., 2010, The Source of the Midwinter Suppression in Storminess over the North Pacific: Journal of Climate, v. 23, n. 3, p. 634–648, https://doi.org/10.1175/2009JCLI2904.1

Petersen, S. V., Defliese, W. F., Saenger, C., Daëron, M., Huntington, K. W., John, C. M., Kelson, J. R., Bernasconi, S. M., Colman, A. S., Kluge, T., Olack, G. A., Schauer, A. J., Bajnai, D., Bonifacie, M., Breitenbach, S. F. M., Fiebig, J., Fernandez, A. B., Henkes, G. A., Hodell, D., Latz, A., Kele, S., Lohmann, K. C., Passey, B. H., Peral, M. Y., Petrizzo, D. A., Rosenheim, B. E., Tripati, A., Venturelli, R., Young, E. D., and Winkelstern, I. Z., 2019, Effects of Improved ^{17}O Correction on Interlaboratory Agreement in Clumped Isotope Calibrations, Estimates of Mineral-Specific Offsets, and Temperature Dependence of Acid Digestion Fractionation: Geochemistry, Geophysics, Geosystems, v. 20, n. 7, p. 3495–3519, https://doi.org/10.1029/2018GC008127

Poage, M. A., and Chamberlain, C. P., 2001, Empirical relationships between elevation and the stable isotope composition of precipitation and surface waters: Considerations for studies of paleoelevation change: American Journal of Science, v. 301, n. 1, p. 1–15, https://doi.org/10.2475/ajs.301.1.1

Putman, A. L., Fiorella, R. P., Bowen, G. J., and Cai, Z., 2019, A Global Perspective on Local Meteoric Water Lines: Meta-analytic Insight Into Fundamental Controls and Practical Constraints: Water Resources Research, v. 55, n. 8, p. 6896–6910, https://doi.org/10.1029/2019WR025181

Quade, J., Cerling, T. E., and Bowman, J. R., 1989, Development of the Asian monsoon revealed by marked ecological shift during the latest Miocene in northern Pakistan: Nature, v. 342, p. 163–166, https://doi.org/10.1038/342163a0

Quade, J., Leary, R., Dettinger, M. P., Orme, D., Krupa, A., DeCelles, P. G., Kano, A., Kato, H., Waldrip, R., Huang, W., and Kapp, P., 2020, Resetting Southern Tibet: The serious challenge of obtaining primary records of Paleoaltimetry: Global and Planetary Change, v. 191, 103194, https://doi.org/10.1016/j.gloplacha.2020.103194

Rea, D. K., Snoeckx, H., and Joseph, L. H., 1998, Late Cenozoic eolian deposition in the North Pacific: Asian drying, Tibetan uplift, and cooling of the northern hemisphere: Paleoceanography, v. 13, n. 3, p. 215–224, https://doi.org/10.1029/98PA00123

Roe, G. H., 2009, On the interpretation of Chinese loess as a paleoclimate indicator: Quaternary Research, v. 71, n. 2, p. 150–161, https://doi.org/10.1016/j.yqres.2008.09.004

Rowley, D. B., Pierrehumbert, R. T., and Currie, B. S., 2001, A new approach to stable isotope-based paleoaltimetry: implications for paleoaltimetry and paleohypsometry of the High Himalaya since the Late Miocene: Earth and Planetary Science Letters, v. 188, n. 1–2, p. 253–268, https://doi.org/10.1016/S0012-821X(01)00324-7

Rugenstein, J. K. C., and Chamberlain, C. P., 2018, The evolution of hydroclimate in Asia over the Cenozoic: A stable-isotope perspective: Earth-Science Reviews, v. 185, p. 1129–1156, https://doi.org/10.1016/j.earscirev.2018.09.003

San Jose, M., Caves Rugenstein, J. K., Cosentino, D., Faccenna, C., Fellin, M. G., Ghinassi, M., and Martini, I., 2020, Stable isotope evidence for rapid uplift of the central Apennines since the late Pliocene: Earth and Planetary Science Letters, v. 544, 116376, https://doi.org/10.1016/j.epsl.2020.116376

Sato, T., Tsujimura, M., Yamanaka, T., Iwasaki, H., Sugimoto, A., Sugita, M., Kimura, F., Davaa, G., and Oyunbaatar, D., 2007, Water sources in semiarid northeast Asia as revealed by field observations and isotope transport model: Journal of Geophysical Research: Atmospheres, v. 112, n. D17, D17112, https://doi.org/10.1029/2006JD008321

Schiemann, R., Lüthi, D., and Schär, C., 2009, Seasonality and Interannual Variability of the Westerly Jet in the Tibetan Plateau Region: Journal of Climate, v. 22, n. 11, p. 2940–2957, https://doi.org/10.1175/2008JCLI2625.1

Shao, Y., and Dong, C. H., 2006, A review on East Asian dust storm climate, modelling and monitoring: Global and Planetary Change, v. 52, n. 1–4, p. 1–22, https://doi.org/10.1016/j.gloplacha.2006.02.011

Shaw, T. A., Baldwin, M., Barnes, E. A., Caballero, R., Garfinkel, C. I., Hwang, Y.-T., Li, C., O'Gorman, P. A., Rivière, G., Simpson, I. R., and Voigt, A., 2016, Storm track processes and the opposing influences of climate change: Nature Geoscience, v. 9, p. 656–664, https://doi.org/10.1038/ngeo2783

Smith, S. G., Wegmann, K. W., Ancuta, L. D., Gosse, J. C., and Hopkins, C. E., 2016, Paleotopography and erosion rates in the central Hangay Dome, Mongolia: Landscape evolution since the mid-Miocene: Journal of Asian Earth Sciences, v. 125, p. 37–57, https://doi.org/10.1016/j.jseaes.2016.05.013

Stein, A. F., Draxler, R. R., Rolph, G. D., Stunder, B. J. B., Cohen, M. D., and Ngan, F., 2015, NOAA's HYSPLIT atmospheric transport and dispersion modeling system: Bulletin of the American Meteorological Society, v. 96, n. 12, p. 2059–2077, https://doi.org/10.1175/BAMS-D-14-00110.1

Still, C. J., Berry, J. A., Collatz, G. J., and DeFries, R. S., 2003, Global distribution of C_3 and C_4 vegetation: Carbon cycle implications: Global Biogeochemical Cycles, v. 17, n. 1, p.6–1–6–14, https://doi.org/10.1029/2001GB001807

Su, T., Farnsworth, A., Spicer, R. A., Huang, J., Wu, F.-X., Liu, J., Li, S.-F., Xing, Y.-W., Huang, Y.-J., Deng, W.-Y.-D., Tang, H., Xu, C.-L., Zhao, F., Srivastava, G., Valdes, P. J., Deng, T., and Zhou, Z.-K., 2019, No

High Tibetan Plateau Until the Neogene: Science Advances, v. 5, n. 3, p. eaav2189, https://doi.org/10.1126/sciadv.aav2189

Sun, J., Gong, Z., Tian, Z., Jia, Y., and Windley, B., 2015, Late Miocene stepwise aridification in the Asian interior and the interplay between tectonics and climate: Palaeogeography, Palaeoclimatology, Palaeoecology, v. 421, p. 48–59, https://doi.org/10.1016/j.palaeo.2015.01.001

Sun, C., Chen, Y., Li, W., Li, X., and Yang, Y., 2016, Isotopic time series partitioning of streamflow components under regional climate change in the Urumqi River, northwest China: Hydrological Sciences Journal, v. 61, n. 8, p. 1443–1459, https://doi.org/10.1080/02626667.2015.1031757

Tian, L., Yao, T., MacClune, K., White, J. W. C., Schilla, A., Vaughn, B., Vachon, R., and Ichiyanagi, K., 2007, Stable isotopic variations in west China: A consideration of moisture sources: Journal of Geophysical Research: Atmosphere, v. 112, n. D10, D10112, https://doi.org/10.1029/2006JD007718

Traynor, J. J., and Sladen, C., 1995, Tectonic and stratigraphic evolution of the Mongolian People's Republic and its influence on hydrocarbon geology and potential: Marine and Petroleum Geology, v. 12, n. 1, p. 35–52, https://doi.org/10.1016/0264-8172(95)90386-X

Wacker, U., Fiebig, J., and Schoene, B. R., 2013, Clumped isotope analysis of carbonates: comparison of two different acid digestion techniques: Rapid Communications in Mass Spectrometry, v. 27, n. 14, p. 1631–1642, https://doi.org/10.1002/rcm.6609

Wacker, U., Fiebig, J., Tödter, J., Schöne, B. R., Bahr, A., Friedrich, O., Tütken, T., Gischler, E., and Joachimski, M. M., 2014, Empirical calibration of the clumped isotope paleothermometer using calcites of various origins: Geochimica et Cosmochimica Acta, v. 141, p. 127–144, https://doi.org/10.1016/j.gca.2014.06.004

Wang, Z., Schauble, E. A., and Eiler, J. M., 2004, Equilibrium thermodynamics of multiply substituted isotopologues of molecular gases: Geochimica et Cosmochimica Acta, v. 68, n. 23, p. 4779–4797, https://doi.org/10.1016/j.gca.2004.05.039

Wheeler, L. B., and Galewsky, J., 2017, Atmospheric Flow Patterns Around the Southern Alps of New Zealand and Implications for Paleoaltimetry: Geophysical Research Letters, v. 44, n. 22, p. 11601–11605, https://doi.org/10.1002/2017GL074753

White, R. H., Battisti, D. S., and Roe, G. H., 2017, Mongolian Mountains Matter Most: Impacts of the Latitude and Height of Asian Orography on Pacific Wintertime Atmospheric Circulation: Journal of Climate, v. 30, n. 11, p. 4065–4082, https://doi.org/10.1175/JCLI-D-16-0401.1

Winnick, M. J., Chamberlain, C. P., Caves, J. K., and Welker, J. M., 2014, Quantifying the isotopic 'continental effect': Earth and Planetary Science Letters, v. 406, p. 123–133, https://doi.org/10.1016/j.epsl.2014.09.005

Wu, H., Wu, J., Song, F., Abuduwaili, J., Saparov, A. S., Chen, X., and Shen, B., 2019, Spatial distribution and controlling factors of surface water stable isotope values ($\delta^{18}O$ and $\delta^{2}H$) across Kazakhstan, Central Asia: Science of the Total Environment, v. 678, p. 53–61, https://doi.org/10.1016/j.scitotenv.2019.03.389

Yamanaka, T., Tsujimura, M., Oyunbaatar, D., and Davaa, G., 2007, Isotopic variation of precipitation over eastern Mongolia and its implication for the atmospheric water cycle: Journal of Hydrology, v. 333, n. 1, p. 21–34, https://doi.org/10.1016/j.jhydrol.2006.07.022

Yuan, W., Carter, A., Dong, J., Bao, Z., An, Y., and Guo, Z., 2006, Mesozoic–Tertiary exhumation history of the Altai Mountains, northern Xinjiang, China: New constraints from apatite fission track data: Tectonophysics, v. 412, n. 3–4, p. 183–193, https://doi.org/10.1016/j.tecto.2005.09.007